ESAIM: M2AN 60 (2026) 411–444
https://doi.org/10.1051/m2an/2026005

ESAIM: Mathematical Modelling and Numerical Analysis
www.esaim-m2an.org

NITSCHE STABILIZED VIRTUAL ELEMENT APPROXIMATIONS FOR A BRINKMAN PROBLEM WITH MIXED BOUNDARY CONDITIONS

David Mora[1,2,**], Jesus Vellojin[3,**] and Nitesh Verma[1,*]

Abstract. In this paper, we formulate, analyze, and implement the discrete formulation of the Brinkman problem with mixed boundary conditions, including slip boundary condition, using the Nitsche's technique for virtual element methods. We propose a discretization by means of the virtual elements presented in Beirão da Veiga *et al.* [*ESAIM Math. Model. Numer. Anal.* **51** (2017) 509–535]. We derive a robust stability analysis of the Nitsche stabilized discrete scheme for this model problem. We establish optimal *a priori* error estimates of the discrete scheme with constants independent of the viscosity. Moreover, a set of numerical tests demonstrates the robustness with respect to the physical parameters and verifies the derived convergence results.

Mathematics Subject Classification. 35Q35, 65N15, 65N22, 65N30, 76D07.

Received June 11, 2024. Accepted January 13, 2026.

1. Introduction and problem statement

We are interested in the numerical approximation by the virtual element method of the Brinkman system with mixed boundary conditions, that is, Dirichlet conditions on one part of the boundary and slip conditions on the rest of the boundary. These boundary conditions, representing the inflow/outflow in the domain, and flow through the boundary wall, as well as fluid slipping along the boundary wall, have been introduced in several applications such as water treatment, reverse osmosis, and so on. The Brinkman equations can be seen as an extension of Darcy's law to describe the laminar flow behavior of a viscous fluid within a porous material with possibly heterogeneous permeability, so that the flow is dominated by the Darcy regime on a part of the domain and by Stokes on the other parts of the domain. In recent years, the numerical solution of this system has acquired great interest due to its high practical importance in different areas, including several industrial and environmental applications, such as filtering porous layers, oil reservoirs, and the study of foams, among others.

The virtual element method (VEM) introduced in [7] belongs to the so-called polytopal methods for solving PDEs by using general polygonal/polyhedral meshes. These methods have received substantial attention in recent years, for instance, hybrid high order method [16, 27–29], discontinuous Galerkin method [4, 21, 48],

Keywords and phrases. Brinkman equation, slip boundary condition, virtual element methods, Nitsche method, *a priori* error analysis, numerical experiments.

[1] GIMNAP, Departamento de Matemática, Universidad del Bío-Bío, Concepción, Chile.

[2] CI^{2}MA, Universidad de Concepción, Concepción, Chile.

[3] Departamento de Ciencias, Universidad Técnica Federico Santa María, Valparaíso, Chile.

*Corresponding author: Nitesh Verma `nverma@ubiobio.cl`

**Other authors who contributed: David Mora `dmora@ubiobio.c`; Jesus Vellojin `jesus.vellojinm@usm.cl`

mimetic finite difference method [8], virtual element method [5, 12, 36] The VEM can be seen as an extension of Finite Elements Method (FEM) to polygonal or polyhedral decompositions. The VEM has been applied to different problems in fluid mechanics, see, for instance, [3, 9–11, 19, 20, 31, 32, 40, 45] and the references therein.

In [32], the virtual element method for a pseudostress-velocity formulation of the nonlinear Brinkman flow has been introduced. The stream virtual element method has been introduced and analyzed in [40]. In this case, the problem is written as a single equation in terms of the stream function of the velocity field by using the incompressibility condition, and optimal error estimates, independent of the viscosity parameter, are obtained. In [9, 10], the authors have introduced a novel divergence-free virtual element method for solving the Stokes and Navier–Stokes problems. This method has been used in [45] for solving the Brinkman problem with homogeneous Dirichlet boundary conditions, and the error estimates, independent of the model parameters, are obtained. Moreover, we also mention recent works on the numerical discretization of the Brinkman problem by finite element methods [1, 2, 30, 39].

The so-called Nitsche methods can be regarded as a stabilization technique where some terms are added to the variational formulation so that the boundary conditions can be incorporated in a weak form. One of the main advantages of the Nitsche method is its versatility. It can be applied to a wide range of partial differential equations, including elliptic, parabolic, and hyperbolic equations. For instance, finite element discretizations with the Nitsche method have evolved to handle general boundary conditions [37], including interface problems [35], unilateral and frictional contact [23, 24], or membrane filtration processes [22], among others. On each reference, we observe that properly formulated penalty terms in the Nitsche method ensure consistency and stability of the numerical solution, even for complex problems and irregular domains. This stability property is crucial for obtaining reliable and accurate results in practical simulations. Moreover, the Nitsche method can be relatively straightforward to implement compared to other approaches for enforcing boundary conditions. Its penalty-based formulation simplifies the incorporation of boundary conditions into the variational formulation of the problem. By the nature of the method, this can be seamlessly integrated with modern numerical techniques such as adaptive mesh refinement, parallel computing, higher-order finite elements, or the virtual elements method. In the latter, the literature regarding Nitsche's method is scarce, with recent contributions by Beirão da Veiga *et al.* [13] and Bertoluzza *et al.* [14]. Here, the authors study the extension to virtual elements of the Lagrange multiplier method, in its stabilized formulation as proposed by Barbosa and Hughes [6], and the Nitsche method [41]. They proved stability and optimal error estimates under custom conditions on the stabilization parameters. The results are extended for two and three-dimensional geometries with curved domains, where the numerical experiments assess the performance of the method, suggesting a viable alternative to the corresponding scheme in the finite element method.

In the present contribution, we propose a Nitsche method for the Brinkman system with mixed boundary conditions. We consider the Dirichlet condition on a part of the boundary and the slip conditions on the rest of the boundary. This approach has been employed in several Navier–Stokes models to impose a slip boundary condition. For example, we have the work from [44], where they compare the Lagrange multiplier and Nitsche's methods for the weak imposition of the slip boundary condition on curved domains. Recently, in [34], the authors studied the weak imposition of the slip boundary through Nitsche's method. They used projected normals, which consist in defining a normal $\mathbf{n}_\pi(\mathbf{x}) = \mathbf{n}(\pi(\mathbf{x}))$, where $\pi(\mathbf{x})$ is an orthogonal projection from the computational to the continuous boundary in order to get the closest point on the continuous boundary. The type of conditions behind the models presented in the aforementioned works is important in different areas for fluid flow problems. In particular, these boundary conditions appear naturally in the analysis of numerical methods for desalination processes, filtration, among others. For that reason, in this work, we extend the results presented in [45] for the new model problem. Unlike the Dirichlet boundary conditions, the slip-boundary conditions are inadequate to impose strongly for a discrete solution. This drawback is due to the unavailability of the degrees of freedom for the normal component and normal derivative of the function on the boundary in the discrete space. It is well-known that different strategies can be considered for imposing mixed conditions, including slip conditions, such as the Lagrange multiplier method. However, we propose here a symmetric discrete variational formulation by adding Nitsche terms in order to incorporate the boundary conditions considered in the model

problem. Moreover, we discretize the problem by using the virtual element method presented in [9] for the Stokes problem. We note that the VEM spaces are based on a divergence conforming virtual element spaces for the velocity and piecewise polynomials for pressure. We define a new Nitsche term to impose the slip boundary condition for the discrete scheme using the piecewise polynomial projection on each polygon K (in the mesh) on the boundary. We mention that in the resulting scheme, the divergence-free property is lost because of the incorporation of the new Nitsche terms. We establish that the discrete problem is well-posed by proving a global inf-sup condition, and we establish stability by using appropriate mesh-parameter dependent norms. Under rather mild assumptions on the polygonal meshes and by using interpolation estimates, the convergence rate is proved to be optimal in terms of the mesh size h. We would like to emphasize that the constants in the derivation of error estimates are independent of the physical parameters in this model problem. The trace inequality for the piecewise polynomials is utilized in the analysis in order to prove the stability. In summary, the advantages of the proposed VEM method with the Nitsche technique to solve the Brinkman problem are: the possibility of using general polygonal meshes, the robustness of error analysis with respect to physical constants, and the possibility of an easy imposition of general boundary conditions, including non-homogeneous Dirichlet conditions, slip conditions, among others.

The rest of the paper is organized as follows: in Section 2, we introduce the variational formulation of the Brinkman equations with mixed boundary conditions. In Section 3 we present the virtual element discretization of arbitrary order $k \geq 2$ with Nitsche's technique. The existence, uniqueness and stability results of the discrete formulation by using a global inf-sup condition are presented in Section 4. In Section 5 we obtain error estimates for the velocity and pressure fields. Section 6 is devoted to analyze, through several numerical experiments, the performance and robustness of the proposed Nitsche method.

In this article, we will employ standard notations for Sobolev spaces, norms and seminorms. In addition, we will denote by C a generic constant independent of the mesh parameter h and model parameters, which may take different values in different occurrences.

2. Governing equations

Let Ω be an open, bounded subset of $\mathbb{R}^2$ having Lipschitz–continuous boundary, such that $\partial\Omega = \bar{\Gamma}_D \cup \bar{\Gamma}_N$, and $\Gamma_D \cap \Gamma_N = \emptyset$. The boundary subdomain Γ_D represents a part of $\partial\Omega$ where a fixed value for the velocity (Dirichlet boundary) is given, while Γ_N denotes a subdomain where we have a slip boundary condition. An example of such a domain is depicted in Figure 1. Thus, the system of interest can be written as the following problem. Given the body force $\boldsymbol{f} \in [L^2(\Omega)]^2$ and boundary condition $\boldsymbol{g} \in [H^{1/2}(\Gamma_D)]^2$, find the fluid velocity $\boldsymbol{u}$ and fluid pressure p, such that

$$\mathbb{K}^{-1}\boldsymbol{u} - \nu \operatorname{div}(\boldsymbol{\varepsilon}(\boldsymbol{u})) + \nabla p = \boldsymbol{f} \qquad \text{in } \Omega, \tag{2.1}$$

$$\nabla \cdot \boldsymbol{u} = 0 \qquad \text{in } \Omega, \tag{2.2}$$

$$\boldsymbol{u} = \boldsymbol{g} \qquad \text{on } \Gamma_D, \tag{2.3}$$

$$(\nu\boldsymbol{\varepsilon}(\boldsymbol{u})\boldsymbol{n}) \cdot \boldsymbol{t} = 0, \quad \text{and} \quad \boldsymbol{u} \cdot \boldsymbol{n} = 0 \qquad \text{on } \Gamma_N, \tag{2.4}$$

where ν is the viscosity of the fluid, $\boldsymbol{\varepsilon}(\boldsymbol{v}) := \frac{1}{2}(\nabla\boldsymbol{v} + (\nabla\boldsymbol{v})^t)$ is the symmetric derivative (here $(\cdot)^t$ denotes transpose), $\mathbb{K}$ is a bounded, symmetric, and positive definite tensor describing the permeability properties of the Brinkman region, and $\boldsymbol{n} := (n_1, n_2)^t$ and $\boldsymbol{t}$ are unit normal and tangent on the boundary Γ_N, respectively, with $\boldsymbol{t} := (-n_2, n_1)^t$.

In order to obtain the weak form of the governing equations, let us introduce the functional spaces for the velocity and pressure as,

$$\mathbf{V} := \{\boldsymbol{v} \in [H^1(\Omega)]^2 : \boldsymbol{v} \cdot \boldsymbol{n} = 0 \text{ on } \Gamma_N, \boldsymbol{v} = \mathbf{0} \text{ on } \Gamma_D\} \qquad \text{and} \qquad Q := L^2_0(\Omega).$$

We first state assumptions on the physical parameters used throughout this paper.

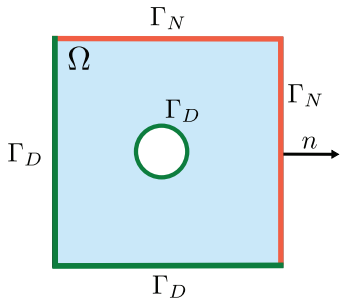

FIGURE 1. Sample geometry of the considered Brinkman domain with mixed boundary conditions.

The permeability tensor holds the positive definiteness, that is, there exist $\kappa_1, \kappa_2 > 0$ for all $\boldsymbol{v} \in \mathbf{V}$ such that

$$0 < \kappa_1 \|\boldsymbol{v}\|_{0,\Omega}^2 \leq (\mathbb{K}^{-1}\boldsymbol{v}, \boldsymbol{v})_{0,\Omega} \leq \kappa_2 \|\boldsymbol{v}\|_{0,\Omega}^2 < \infty,$$

and we also assume that $0 < \nu \leq \nu_{\max}$.

Next, we test the corresponding equations in (2.1) and (2.2) and using integration by parts and the fact that $\boldsymbol{v} \in \mathbf{V}$, we have

$$\begin{aligned} \int_\Omega \mathbb{K}^{-1}\boldsymbol{u} \cdot \boldsymbol{v} + \nu \int_\Omega \boldsymbol{\varepsilon}(\boldsymbol{u}) : \boldsymbol{\varepsilon}(\boldsymbol{v}) - \int_\Omega p \operatorname{div} \boldsymbol{v} - \int_{\Gamma_N} (\nu\boldsymbol{\varepsilon}(\boldsymbol{u}) - p\mathbb{I})\boldsymbol{n} \cdot \boldsymbol{v}\, \mathrm{d}s = \int_\Omega \boldsymbol{f} \cdot \boldsymbol{v} \qquad & \forall \boldsymbol{v} \in \mathbf{V}, \\ - \int_\Omega \operatorname{div} \boldsymbol{u}\, q = 0 \qquad & \forall q \in Q. \end{aligned}$$

To impose the Dirichlet condition for the continuous solution $\boldsymbol{u}$, we define the Sobolev space

$$\mathbf{V}_g := \{\boldsymbol{v} \in \mathbf{V} : \boldsymbol{v} \cdot \boldsymbol{n} = 0 \text{ on } \Gamma_N, \boldsymbol{v} = \boldsymbol{g} \text{ on } \Gamma_D\}.$$

The boundary term in the weak formulation for $\boldsymbol{u} \in \mathbf{V}_g$, $\boldsymbol{v} \in \mathbf{V}$ and $p \in Q$ can be computed by splitting in terms of tangential and normal components ($\boldsymbol{v} = (\boldsymbol{v} \cdot \boldsymbol{n})\boldsymbol{n} + (\boldsymbol{v} \cdot \boldsymbol{t})\boldsymbol{t}$) as,

$$\begin{aligned} \int_{\Gamma_N} (\nu\boldsymbol{\varepsilon}(\boldsymbol{u}) - p\mathbb{I})\boldsymbol{n} \cdot \boldsymbol{v}\, \mathrm{d}s &= \int_{\Gamma_N} \Big((\boldsymbol{n}^t(\nu\boldsymbol{\varepsilon}(\boldsymbol{u})\boldsymbol{n}))(\boldsymbol{v} \cdot \boldsymbol{n}) + (\boldsymbol{t}^t(\nu\boldsymbol{\varepsilon}(\boldsymbol{u})\boldsymbol{n}))(\boldsymbol{v} \cdot \boldsymbol{t}) - p(\boldsymbol{v} \cdot \boldsymbol{n}) \Big)\, \mathrm{d}s \\ &= \int_{\Gamma_N} (\boldsymbol{t}^t(\nu\boldsymbol{\varepsilon}(\boldsymbol{u})\boldsymbol{n}))(\boldsymbol{v} \cdot \boldsymbol{t})\, \mathrm{d}s = 0, \end{aligned}$$

where we have also used the boundary condition (2.4).

Thus, the weak formulation of the problem is stated as: find $\boldsymbol{u} \in \mathbf{V}_g$ and $p \in Q$ such that

$$m(\boldsymbol{u}, \boldsymbol{v}) + a(\boldsymbol{u}, \boldsymbol{v}) + b(\boldsymbol{v}, p) = F(\boldsymbol{v}) \qquad \forall \boldsymbol{v} \in \mathbf{V}, \tag{2.5a}$$

$$b(\boldsymbol{u}, q) = 0 \qquad \forall q \in Q, \tag{2.5b}$$

where the corresponding bilinear forms and the linear functional are introduced as follows

$$\begin{aligned} m(\boldsymbol{u}, \boldsymbol{v}) &:= \int_\Omega \mathbb{K}^{-1}\boldsymbol{u} \cdot \boldsymbol{v}, \qquad a(\boldsymbol{u}, \boldsymbol{v}) := \nu \int_\Omega \boldsymbol{\varepsilon}(\boldsymbol{u}) : \boldsymbol{\varepsilon}(\boldsymbol{v}), \\ b(\boldsymbol{v}, q) &:= - \int_\Omega q \operatorname{div} \boldsymbol{v}, \quad \text{and} \quad F(\boldsymbol{v}) := \int_\Omega \boldsymbol{f} \cdot \boldsymbol{v}. \end{aligned}$$

Now, we introduce the parameter dependent norm for all $\boldsymbol{v} \in \mathbf{V}$ as follows:

$$|||\boldsymbol{v}|||_{\mathbf{V}}^2 := \|\mathbb{K}^{-1/2}\boldsymbol{v}\|_{0,\Omega}^2 + \nu\|\boldsymbol{\varepsilon}(\boldsymbol{v})\|_{0,\Omega}^2 + \|\operatorname{div}\boldsymbol{v}\|_{0,\Omega}^2.$$

Denoting

$$\begin{aligned}\mathcal{A}((\boldsymbol{u},p),(\boldsymbol{v},q)) &:= m(\boldsymbol{u},\boldsymbol{v}) + a(\boldsymbol{u},\boldsymbol{v}) + b(\boldsymbol{v},p) - b(\boldsymbol{u},q),\\ \mathcal{L}(\boldsymbol{v},q) &:= F(\boldsymbol{v}),\end{aligned}$$

then we can rewrite the continuous formulation (2.5) in vector form as: find $(\boldsymbol{u},p) \in \mathbf{V}_g \times Q$ such that

$$\mathcal{A}((\boldsymbol{u},p),(\boldsymbol{v},q)) = \mathcal{L}(\boldsymbol{v},q) \qquad \forall(\boldsymbol{v},q) \in \mathbf{V}\times Q.$$

Defining the kernel space as

$$\mathbf{Z} := \{\boldsymbol{v} \in \mathbf{V} : b(\boldsymbol{v},q) = 0 \quad \forall q \in Q\} = \{\boldsymbol{v} \in \mathbf{V} : \operatorname{div}\boldsymbol{v} = 0\},$$

then we have the following properties of the bilinear forms:

$$\begin{gathered}m(\boldsymbol{u},\boldsymbol{v}) \le |||\boldsymbol{u}|||_{\mathbf{V}}|||\boldsymbol{v}|||_{\mathbf{V}}, \qquad a(\boldsymbol{u},\boldsymbol{v}) \le |||\boldsymbol{u}|||_{\mathbf{V}}|||\boldsymbol{v}|||_{\mathbf{V}} \quad \forall \boldsymbol{u},\boldsymbol{v} \in \mathbf{V},\\ b(\boldsymbol{v},q) \le |||\boldsymbol{v}|||_{\mathbf{V}}\|q\|_Q \quad \forall \boldsymbol{v} \in \mathbf{V}, q \in Q, \qquad F(\boldsymbol{v}) \le \|\boldsymbol{f}\|_{\mathbf{V}^*}|||\boldsymbol{v}|||_{\mathbf{V}} \quad \forall \boldsymbol{v} \in \mathbf{V},\\ m(\boldsymbol{v},\boldsymbol{v}) + a(\boldsymbol{v},\boldsymbol{v}) \ge |||\boldsymbol{v}|||_{\mathbf{V}}^2 \quad \forall \boldsymbol{v} \in \mathbf{Z}, \quad \text{and} \quad \text{there exist } \beta > 0 \text{ s.t. } \sup_{(0\neq)\boldsymbol{v}\in\mathbf{V}} \frac{b(\boldsymbol{v},q)}{|||\boldsymbol{v}|||_{\mathbf{V}}} \ge \beta\|q\|_Q \qquad \forall q \in Q,\end{gathered}$$

where $\|q\|_Q := \|q\|_{0,\Omega}$ and $\|\boldsymbol{f}\|_{\mathbf{V}^*} := \sup_{(0\neq)\boldsymbol{v}\in\mathbf{V}} \frac{F(\boldsymbol{v})}{|||\boldsymbol{v}|||_{\mathbf{V}}}$.

Using the ellipticity of $m(\cdot,\cdot)+a(\cdot,\cdot)$ on $\mathbf{Z}$, and the inf-sup condition of $b(\cdot,\cdot)$, and continuity of the bilinear forms of $m(\cdot,\cdot)$, $a(\cdot,\cdot)$, $b(\cdot,\cdot)$ and continuity of the linear functional $F(\cdot)$, we have the well posedness of the weak formulation (2.5) (refer [15,17]).

Lemma 2.1. *The continuous solution $(\boldsymbol{u},p) \in \mathbf{V}_g \times Q$ of formulation (2.5) holds the following bound, for a constant C (independent of ν, $\mathbb{K}$),*

$$|||\boldsymbol{u}|||_{\mathbf{V}} + \|p\|_Q \le C\|\boldsymbol{f}\|_{\mathbf{V}^*}.$$

3. Virtual element approximation

In this section we construct a VEM for solving the Brinkman problem with mixed boundary conditions using Nitsche's technique. We start denoting by $\{\mathcal{T}_h\}_{h>0}$ a sequence of partitions into polygons of the domain Ω. The elements in $\mathcal{T}_h$ are denoted as K, and edges by e. Let h_K denote the diameter of the element K and $h := \max_{K\in\mathcal{T}_h} h_K$ the maximum of the diameters of all the elements of the mesh. By N_K^v we denote the number of vertices in the polygon K, N_K^e stands for the number of faces on ∂K, and e is a generic edge of $\mathcal{T}_h$. We denote by $\boldsymbol{n}_K^e$ the unit normal pointing outwards K and by $\boldsymbol{t}_K^e$ the unit tangent vector along e on K, and V_i represents the i^{th} vertex of the polygon K.

Next, we denote the sets of all boundary edges as $\mathcal{E}_h(\Omega)$ and denote the edges on the Dirichlet boundary as $\mathcal{E}_h^D := \Gamma_D \cap \mathcal{E}_h(\Omega)$ and edges on the other boundary as $\mathcal{E}_h^N := \Gamma_N \cap \mathcal{E}_h(\Omega)$.

In addition, for the theoretical analysis we will make the following assumptions: there exists $C_{\mathcal{T}} > 0$ such that, for every h and every $K \in \mathcal{T}_h$, (a) the ratio between the shortest edge and h_K is larger than $C_{\mathcal{T}}$; and (b) $K \in \mathcal{T}_h$ is star-shaped with respect to every point within a ball of radius $C_{\mathcal{T}}h_K$.

In what follows, we denote by $\mathbb{P}_k(K)$, the space of polynomials of degree up to k, defined locally on $K \in \mathcal{T}_h$. Moreover, we denote by $\mathcal{G}_k(K) := \nabla(\mathbb{P}_{k+1}(K)) \subseteq [\mathbb{P}_k(K)]^2$ and $\mathcal{G}_k^{\perp}(K) \subseteq [\mathbb{P}_k(K)]^2$ the L^2-orthogonal complement to $\mathcal{G}_k(K)$.

3.1. Discrete spaces and degrees of freedom

The local virtual element spaces are defined for $k \geq 2$ as,

$$\tilde{\mathbf{V}}_h^k(K) := \big\{\boldsymbol{v} \in [H^1(K) \cap C^0(\partial K)]^2 : -\boldsymbol{\Delta}\boldsymbol{v} - \nabla s \in \mathcal{G}_{k-2}(K)^\perp (\text{for some } s \in L^2(K)), \quad \operatorname{div}\boldsymbol{v} \in \mathbb{P}_{k-1}(K), \\ \boldsymbol{v}|_e \in \mathbb{P}_k(e)\,\forall e \in \partial K\big\},$$

$$Q_h^{k-1}(K) := \mathbb{P}_{k-1}(K).$$

Denote the dimension of local space $\tilde{\mathbf{V}}_h^k(K)$ as $N_{\mathbf{V}}^K$, and dimension of $Q_h^{k-1}(K)$ as N_Q^K.
The local degrees of freedom ($\text{dof}_i^{\mathbf{V}}$, $1 \leq i \leq N_{\mathbf{V}}^K$) for space $\tilde{\mathbf{V}}_h^k(K)$ for a generic $\boldsymbol{v}_h \in \tilde{\mathbf{V}}_h^k(K)$ are given by

- the values of $\boldsymbol{v}_h$ at the vertices of the polygon K,
- the values of $\boldsymbol{v}_h$ at $k-1$ points in the interior of edges $e \in \partial K$,
- the moments of $\boldsymbol{v}_h$

$$\int_K \boldsymbol{v}_h \cdot \boldsymbol{g}_{k-2}^\perp \quad \text{for all } \boldsymbol{g}_{k-2}^\perp \in \mathcal{G}_{k-2}(K)^\perp,$$

- for $k > 1$, the moments of $\operatorname{div}\boldsymbol{v}_h$ in K,

$$\int_K \operatorname{div}\boldsymbol{v}_h\, q_{k-1} \quad \text{for all } q_{k-1} \in \mathbb{P}_{k-1}(K).$$

And for the space $Q_h^{k-1}(K)$, the degrees of freedom are

- the moments of q_h

$$\int_K q_h\, z_{k-1} \quad \text{for all } z_{k-1} \in \mathbb{P}_{k-1}(K).$$

Denoting the bilinear forms on each element as $a^K(\cdot,\cdot) := a(\cdot,\cdot)|_K$ for any bilinear form, we introduce the energy projection operators $\boldsymbol{\Pi}_K^{\nabla,k} : [H^1(K)]^2 \to [\mathbb{P}_k(K)]^2, \boldsymbol{\Pi}_K^{\boldsymbol{\epsilon},k} : [H^1(K)]^2 \to [\mathbb{P}_k(K)]^2$, and L^2 projection operator $\boldsymbol{\Pi}_K^{\mathbf{0},k} : [L^2(K)]^2 \to [\mathbb{P}_k(K)]^2$ for all $K \in \mathcal{T}_h$ to define the computable bilinear forms,

$$\forall \boldsymbol{v} \in \big[H^1(K)\big]^2, \begin{cases} \Big(\boldsymbol{\nabla}\Big(\boldsymbol{\Pi}_K^{\nabla,k}\boldsymbol{v} - \boldsymbol{v}\Big), \boldsymbol{\nabla}\boldsymbol{r}_k\Big) = 0 \quad \forall \boldsymbol{r}_k \in [\mathbb{P}_k(K)]^2, \\ P_K^0\Big(\boldsymbol{\Pi}_K^{\nabla,k}\boldsymbol{v} - \boldsymbol{v}\Big) = \mathbf{0} \end{cases} \tag{3.1}$$

$$\forall \boldsymbol{v} \in [H^1(K)]^2, \begin{cases} a^K\Big(\boldsymbol{\Pi}_K^{\boldsymbol{\epsilon},k}\boldsymbol{v} - \boldsymbol{v}, \boldsymbol{r}_k\Big) = 0 \quad \forall \boldsymbol{r}_k \in [\mathbb{P}_k(K)]^2, \\ \Big(\boldsymbol{\Pi}_K^{\boldsymbol{\epsilon},k}\boldsymbol{v} - \boldsymbol{v}, \boldsymbol{r}_k\Big)_{0,K} = \mathbf{0} \quad \forall \boldsymbol{r}_k \in \ker\big(a^K(\cdot,\cdot)\big), \end{cases} \tag{3.2}$$

$$\forall \boldsymbol{v} \in \big[L^2(K)\big]^2, \quad \Big(\boldsymbol{\Pi}_K^{\mathbf{0},k}\boldsymbol{v} - \boldsymbol{v}, \boldsymbol{r}_k\Big)_{0,K} = 0 \qquad \forall \boldsymbol{v} \in \big[L^2(K)\big]^2, \boldsymbol{r}_k \in [\mathbb{P}_k(K)]^2, \tag{3.3}$$

where P_K^0 is projection onto constants.

Refer to [45], we utilize the modified virtual element space for fluid velocity with the help of energy projection (3.1) as,

$$\mathbf{V}_h^k(K) := \Big\{\boldsymbol{v} \in \big[H^1(K) \cap C^0(\partial K)\big]^2 : -\boldsymbol{\Delta}\boldsymbol{v} - \nabla s \in \mathcal{G}_k(K)^\perp \quad \text{for some } s \in L^2(K), \\ \operatorname{div}\boldsymbol{v} \in \mathbb{P}_{k-1}(K), \quad \boldsymbol{v}|_e \in \mathbb{P}_k(e)\,\forall e \in \partial K, \\ \Big(\boldsymbol{\Pi}_K^{\nabla,k}\boldsymbol{v} - \boldsymbol{v}, \boldsymbol{g}_{k\backslash k-2}^\perp\Big)_{0,K} = 0 \quad \forall\, \boldsymbol{g}_{k\backslash k-2}^\perp \in \mathcal{G}_k(K)^\perp \backslash \mathcal{G}_{k-2}(K)^\perp\Big\}.$$

The degrees of freedom for the space $\mathbf{V}_h^k(K)$ are same as $\tilde{\mathbf{V}}_h^k(K)$.

Remark 3.1. The space $\mathbf{V}_h^k(K)$ will be useful for computing the L^2-projection (3.3) onto $\mathbb{P}_k(K)$ to approximate the zero order term presented in bilinear form $m(\cdot,\cdot)$.

Remark 3.2. The imposition of Dirichlet boundary condition using the interpolant is not enough with complex domains, and the slip boundary conditions are not easy to impose in numerical experiments. Thus, we proceed here with the Nitsche's technique for mixed boundary imposition.

We introduce the virtual element spaces to be used in the discretization of the Brinkman problem as,

$$\mathbf{V}_h^k := \{\boldsymbol{v}_h \in [H^1(\Omega)]^2 : \boldsymbol{v}_h|_K \in \mathbf{V}_h^k(K)\ \forall K \in \mathcal{T}_h\}, \qquad Q_h^{k-1} := \{q_h \in Q : q_h|_K \in Q_h^{k-1}(K)\ \forall K \in \mathcal{T}_h\}.$$

Thus, the discrete formulation states that we seek the discrete velocity $\boldsymbol{u}_h \in \mathbf{V}_h^k$ and discrete fluid pressure $p_h \in Q_h^{k-1}$ such that the following holds for all $\boldsymbol{v}_h \in \mathbf{V}_h^k$ and $q_h \in Q_h^{k-1}$

$$\begin{aligned}
&\sum_{K\in\mathcal{T}_h}\Big(m^K\Big(\boldsymbol{\Pi}_K^{\mathbf{0},k}\boldsymbol{u}_h,\boldsymbol{\Pi}_K^{\mathbf{0},k}\boldsymbol{v}_h\Big)+\mathcal{S}_K^0\Big(\Big(\mathbf{I}-\boldsymbol{\Pi}_K^{0,k}\Big)\boldsymbol{u}_h,(\mathbf{I}-\boldsymbol{\Pi}_K^{0,k})\boldsymbol{v}_h\Big)\\
&\quad+a^K\Big(\boldsymbol{\Pi}_K^{\boldsymbol{\varepsilon},k}\boldsymbol{u}_h,\boldsymbol{\Pi}_K^{\boldsymbol{\varepsilon},k}\boldsymbol{v}_h\Big)+\mathcal{S}_K^{\boldsymbol{\varepsilon}}\Big(\Big(\mathbf{I}-\boldsymbol{\Pi}_K^{\boldsymbol{\varepsilon},k}\Big)\boldsymbol{u}_h,\Big(\mathbf{I}-\boldsymbol{\Pi}_K^{\boldsymbol{\varepsilon},k}\Big)\boldsymbol{v}_h\Big)\Big)\\
&\quad+\sum_{e\in\mathcal{E}_h^D}\Big(\gamma_D\int_e h_e^{-1}\boldsymbol{u}_h\cdot\boldsymbol{v}_h\,\mathrm{d}s-\int_e\Big(\nu\boldsymbol{\varepsilon}\Big(\Pi_{K_e}^{\boldsymbol{\varepsilon},k}\boldsymbol{u}_h\Big)\boldsymbol{n}\Big)\cdot\boldsymbol{v}_h\,\mathrm{d}s-\int_e\Big(\nu\boldsymbol{\varepsilon}\Big(\Pi_{K_e}^{\boldsymbol{\varepsilon},k}\boldsymbol{v}_h\Big)\boldsymbol{n}\Big)\cdot\boldsymbol{u}_h\,\mathrm{d}s\Big)\\
&\quad+\sum_{e\in\mathcal{E}_h^N}\Big(\gamma_N\int_e h_e^{-1}(\boldsymbol{u}_h\cdot\boldsymbol{n})(\boldsymbol{v}_h\cdot\boldsymbol{n})\,\mathrm{d}s-\int_e\Big(\boldsymbol{n}^t\Big(\nu\boldsymbol{\varepsilon}\Big(\Pi_{K_e}^{\boldsymbol{\varepsilon},k}\boldsymbol{u}_h\Big)\boldsymbol{n}\Big)\Big)(\boldsymbol{v}_h\cdot\boldsymbol{n})\,\mathrm{d}s\\
&\quad-\int_e\Big(\boldsymbol{n}^t\Big(\nu\boldsymbol{\varepsilon}\Big(\Pi_{K_e}^{\boldsymbol{\varepsilon},k}\boldsymbol{v}_h\Big)\boldsymbol{n}\Big)\Big)(\boldsymbol{u}_h\cdot\boldsymbol{n})\,\mathrm{d}s\Big)\\
&\quad+\sum_{K\in\mathcal{T}_h}b^K(\boldsymbol{v}_h,p_h)+\sum_{e\in\mathcal{E}_h^D}\int_e(p_h\boldsymbol{n})\cdot\boldsymbol{v}_h\,\mathrm{d}s+\sum_{e\in\mathcal{E}_h^N}\int_e p_h(\boldsymbol{v}_h\cdot\boldsymbol{n})\,\mathrm{d}s\\
&\quad=\sum_{K\in\mathcal{T}_h}\Big(\boldsymbol{\Pi}_K^{\mathbf{0},k-1}\boldsymbol{f},\boldsymbol{v}_h\Big)_{0,K}+\gamma_D\sum_{e\in\mathcal{E}_h^D}\int_e h_e^{-1}\boldsymbol{g}\cdot\boldsymbol{v}_h\,\mathrm{d}s-\sum_{e\in\mathcal{E}_h^D}\int_e\boldsymbol{g}\cdot\Big(\nu\boldsymbol{\varepsilon}\Big(\Pi_{K_e}^{\boldsymbol{\varepsilon},k}\boldsymbol{v}_h\Big)\boldsymbol{n}\Big)\,\mathrm{d}s,\\
&\sum_{K\in\mathcal{T}_h}b^K(\boldsymbol{u}_h,q_h)+\sum_{e\in\mathcal{E}_h^D}\int_e(q_h\boldsymbol{n})\cdot\boldsymbol{u}_h\,\mathrm{d}s+\sum_{e\in\mathcal{E}_h^N}\int_e q_h(\boldsymbol{u}_h\cdot\boldsymbol{n})\,\mathrm{d}s=\sum_{e\in\mathcal{E}_h^D}\int_e\boldsymbol{g}\cdot(q_h\boldsymbol{n})\,\mathrm{d}s,
\end{aligned}$$

where $\Pi_{K_e}^{\boldsymbol{\varepsilon},k}$ is the projection onto piecewise polynomial on element K_e having boundary containing the edge e.

Introduce the discrete bilinear forms and linear functionals for all $\boldsymbol{u}_h,\boldsymbol{v}_h \in \mathbf{V}_h^k$, $q_h \in Q_h^{k-1}$ as,

$$\begin{aligned}
m_h(\boldsymbol{u}_h,\boldsymbol{v}_h) &:= \sum_{K\in\mathcal{T}_h}\Big(m^K\Big(\boldsymbol{\Pi}_K^{\mathbf{0},k}\boldsymbol{u}_h,\boldsymbol{\Pi}_K^{\mathbf{0},k}\boldsymbol{v}_h\Big)+\mathcal{S}_K^0\Big(\Big(\mathbf{I}-\boldsymbol{\Pi}_K^{0,k}\Big)\boldsymbol{u}_h,\Big(\mathbf{I}-\boldsymbol{\Pi}_K^{0,k}\Big)\boldsymbol{v}_h\Big)\Big),\\
a_h(\boldsymbol{u}_h,\boldsymbol{v}_h) &:= \sum_{K\in\mathcal{T}_h}a_h^K(\boldsymbol{u}_h,\boldsymbol{v}_h)+\mathcal{N}_h^{S,D}(\boldsymbol{u}_h,\boldsymbol{v}_h)+\mathcal{N}_h^{B,D}(\boldsymbol{u}_h,\boldsymbol{v}_h)+\mathcal{N}_h^{B,D}(\boldsymbol{v}_h,\boldsymbol{u}_h)\\
&\quad+\mathcal{N}_h^{S,N}(\boldsymbol{u}_h,\boldsymbol{v}_h)+\mathcal{N}_h^{B,N}(\boldsymbol{u}_h,\boldsymbol{v}_h)+\mathcal{N}_h^{B,N}(\boldsymbol{v}_h,\boldsymbol{u}_h),\\
b_h(\boldsymbol{v}_h,q_h) &:= \sum_{K\in\mathcal{T}_h}b^K(\boldsymbol{v}_h,q_h)+\mathcal{N}_h^{b,D}(\boldsymbol{v}_h,q_h)+\mathcal{N}_h^{b,N}(\boldsymbol{v}_h,q_h),\\
F_h(\boldsymbol{v}_h) &:= \langle\boldsymbol{f}_h,\boldsymbol{v}_h\rangle+\gamma_D\sum_{e\in\mathcal{E}_h^D}\int_e h_e^{-1}\boldsymbol{g}\cdot\boldsymbol{v}_h\,\mathrm{d}s-\sum_{e\in\mathcal{E}_h^D}\int_e\boldsymbol{g}\cdot\Big(\nu\boldsymbol{\varepsilon}\Big(\Pi_{K_e}^{\boldsymbol{\varepsilon},k}\boldsymbol{v}_h\Big)\boldsymbol{n}\Big)\,\mathrm{d}s,\\
&\text{and}\quad G(q_h) := \sum_{e\in\mathcal{E}_h^D}\int_e\boldsymbol{g}\cdot(q_h\boldsymbol{n})\,\mathrm{d}s,
\end{aligned}$$

where $a_h^K(\boldsymbol{u}_h,\boldsymbol{v}_h) := a^K(\boldsymbol{\Pi}_K^{\boldsymbol{\epsilon},k}\boldsymbol{u}_h,\boldsymbol{\Pi}_K^{\boldsymbol{\epsilon},k}\boldsymbol{v}_h) + \mathcal{S}_K^{\boldsymbol{\epsilon}}((\mathbf{I}-\boldsymbol{\Pi}_K^{\boldsymbol{\epsilon},k})\boldsymbol{u}_h,(\mathbf{I}-\boldsymbol{\Pi}_K^{\boldsymbol{\epsilon},k})\boldsymbol{v}_h)$, and $\boldsymbol{f}_h|_K := \boldsymbol{\Pi}_K^{\mathbf{0},k-1}\boldsymbol{f}$.

On the one hand, we note that the stabilization terms $\mathcal{S}_K^{\boldsymbol{\epsilon}}(\cdot,\cdot),\mathcal{S}_K^0(\cdot,\cdot)$ are defined, for all $\boldsymbol{v}_h \in \mathbf{V}_h^k(K)$, so that we have the stability with respective bilinear forms, for constants $\zeta_1,\zeta_2,\xi_1,\xi_2 > 0$, independent of h and any physical parameters,

$$\zeta_1\, a^K(\boldsymbol{v}_h,\boldsymbol{v}_h) \le \mathcal{S}_K^{\boldsymbol{\epsilon}}(\boldsymbol{v}_h,\boldsymbol{v}_h) \le \zeta_2\, a^K(\boldsymbol{v}_h,\boldsymbol{v}_h), \text{ and } \xi_1 m^K(\boldsymbol{v}_h,\boldsymbol{v}_h) \le \mathcal{S}_K^0(\boldsymbol{v}_h,\boldsymbol{v}_h) \le \xi_2\, m^K(\boldsymbol{v}_h,\boldsymbol{v}_h). \tag{3.4}$$

On the other hand, the Nitsche's stabilization terms with parameter $\gamma_D,\gamma_N > 0$, $\forall \boldsymbol{v}_h \in \mathbf{V}_h^k$, $q_h \in Q_h^{k-1}$ as

$$\mathcal{N}_h^{S,D}(\boldsymbol{u}_h,\boldsymbol{v}_h) := \gamma_D \sum_{e\in\mathcal{E}_h^D}\int_e h_e^{-1}\boldsymbol{u}_h\cdot\boldsymbol{v}_h\,\mathrm{d}s, \qquad \mathcal{N}_h^{B,D}(\boldsymbol{u}_h,\boldsymbol{v}_h) := -\sum_{e\in\mathcal{E}_h^D}\int_e\Big(\nu\boldsymbol{\varepsilon}\Big(\Pi_{K_e}^{\boldsymbol{\epsilon},k}\boldsymbol{u}_h\Big)\boldsymbol{n}\Big)\cdot\boldsymbol{v}_h\,\mathrm{d}s,$$

$$\mathcal{N}_h^{b,D}(\boldsymbol{v}_h,q_h) := \sum_{e\in\mathcal{E}_h^D}\int_e (q_h\boldsymbol{n})\cdot\boldsymbol{v}_h\,\mathrm{d}s, \qquad \mathcal{N}_h^{S,N}(\boldsymbol{u}_h,\boldsymbol{v}_h) := \gamma_N\sum_{e\in\mathcal{E}_h^N}\int_e h_e^{-1}(\boldsymbol{u}_h\cdot\boldsymbol{n})(\boldsymbol{v}_h\cdot\boldsymbol{n})\,\mathrm{d}s,$$

$$\mathcal{N}_h^{B,N}(\boldsymbol{u}_h,\boldsymbol{v}_h) := -\sum_{e\in\mathcal{E}_h^N}\int_e\Big(\boldsymbol{n}^t\Big(\nu\boldsymbol{\varepsilon}\Big(\Pi_{K_e}^{\boldsymbol{\epsilon},k}\boldsymbol{u}_h\Big)\boldsymbol{n}\Big)\Big)(\boldsymbol{v}_h\cdot\boldsymbol{n})\,\mathrm{d}s, \quad \text{and} \quad \mathcal{N}_h^{b,N}(\boldsymbol{v}_h,q_h) := \sum_{e\in\mathcal{E}_h^N}\int_e q_h(\boldsymbol{v}_h\cdot\boldsymbol{n})\,\mathrm{d}s.$$

Now, we are in a position to introduce the virtual element formulation with Nitsche stabilization for the Brinkman problem with mixed boundary conditions, as follows: seek $\boldsymbol{u}_h \in \mathbf{V}_h^k$, and $p_h \in Q_h^{k-1}$ such that

$$m_h(\boldsymbol{u}_h,\boldsymbol{v}_h) + a_h(\boldsymbol{u}_h,\boldsymbol{v}_h) + b_h(\boldsymbol{v}_h,p_h) = F_h(\boldsymbol{v}_h) \qquad \forall \boldsymbol{v}_h \in \mathbf{V}_h^k, \tag{3.5a}$$

$$b_h(\boldsymbol{u}_h,q_h) = G(q_h) \qquad \forall q_h \in Q_h^{k-1}. \tag{3.5b}$$

Denoting

$$\mathcal{A}_h((\boldsymbol{u}_h,p_h),(\boldsymbol{v}_h,q_h)) := m_h(\boldsymbol{u}_h,\boldsymbol{v}_h) + a_h(\boldsymbol{u}_h,\boldsymbol{v}_h) + b_h(\boldsymbol{v}_h,p_h) - b_h(\boldsymbol{u}_h,q_h),$$
$$\mathcal{L}_h(\boldsymbol{v}_h,q_h) := F_h(\boldsymbol{v}_h) - G(q_h),$$

then we can rewrite the discrete formulation (3.5a) and (3.5b), in vector form as: find $(\boldsymbol{u}_h,p_h) \in \mathbb{V}_h^k := \mathbf{V}_h^k \times Q_h^{k-1}$ such that

$$\mathcal{A}_h((\boldsymbol{u}_h,p_h),(\boldsymbol{v}_h,q_h)) = \mathcal{L}_h(\boldsymbol{v}_h,q_h) \qquad \forall (\boldsymbol{v}_h,q_h) \in \mathbb{V}_h^k. \tag{3.6}$$

Remark 3.3. The Nitsche stabilization terms in our formulation (3.5), such as, $\mathcal{N}_h^{S,D}(\cdot,\cdot)$ and $\mathcal{N}_h^{S,N}(\cdot,\cdot)$ are used to impose the Dirichlet and slip boundary conditions, respectively, for the discrete solution. The other terms in the formulation, such as, $\mathcal{N}_h^{B,D}(\boldsymbol{u}_h,\boldsymbol{v}_h)$, $\mathcal{N}_h^{B,N}(\boldsymbol{u}_h,\boldsymbol{v}_h)$, $\mathcal{N}_h^{b,D}(\boldsymbol{v}_h,p_h)$,$\mathcal{N}_h^{b,N}(\boldsymbol{v}_h,p_h)$ appears naturally while the terms $\mathcal{N}_h^{B,D}(\boldsymbol{v}_h,\boldsymbol{u}_h)$, $\mathcal{N}_h^{B,N}(\boldsymbol{v}_h,\boldsymbol{u}_h)$, $\mathcal{N}_h^{b,D}(\boldsymbol{u}_h,q_h)$,$\mathcal{N}_h^{b,N}(\boldsymbol{u}_h,q_h)$ are added to retain the symmetry in the discrete formulation.

4. Solvability of the VEM with Nitsche stabilized terms

In this section, we are going to prove the well-posedness of our discrete formulation. First, we state below the preliminary results used further in analysis. We recall the classical trace and inverse inequalities for piecewise polynomials.

Lemma 4.1 (Local trace inequality)**.** *There exists a positive constant C_t such that for $w \in H^\delta(K)$, $\delta \in (1/2,1]$ it holds*

$$\|w\|_{0,\partial K} \le C_t\Big(h_K^{-1/2}\|w\|_{0,K} + h_K^{\delta-1/2}|w|_{\delta,K}\Big), \quad \forall K \in \mathcal{T}_h.$$

Lemma 4.2 (Discrete inverse inequality)**.** *There exists a positive constant C_I such that, for all $w_h \in \mathbb{P}_k(K)$ and $K \in \mathcal{T}_h$, it holds*

$$\|\nabla w_h\|_{0,K} \leq C_I h_K^{-1} \|w_h\|_{0,K}.$$

Lemma 4.3. *The following inequalities hold, with constants $C_{tr} > 0$ and $C_T > 0$ independent of h,*

$$\|q_h\|_{h,D} := \left(\sum_{e \in \mathcal{E}_h^D} h_e \|q_h\|_{0,e}^2 \right)^{1/2} \leq C_{tr} \|q_h\|_{0,\Omega} \qquad \forall q_h \in Q_h^{k-1},$$

$$\left(\sum_{e \in \mathcal{E}_h^D} h_e \left\| \boldsymbol{\varepsilon}\left(\Pi_{K_e}^{\boldsymbol{\varepsilon},k} \boldsymbol{v}_h \right) \boldsymbol{n} \right\|_{0,e}^2 \right)^{1/2} \leq C_T \|\boldsymbol{\varepsilon}(\boldsymbol{v}_h)\|_{0,\Omega} \qquad \forall \boldsymbol{v}_h \in \mathbf{V}_h^k$$

and same holds on the boundary Γ_N.

Proof. Using Lemma 4.1 and Lemma 4.2 and for $C_{\mathrm{tr}} := C_t C_I$, there holds

$$\|q_h\|_{0,\partial K} \leq C_{\mathrm{tr}} h_K^{-1/2} \|q_h\|_{0,K} \quad \forall q_h \in Q_h^{k-1}.$$

Using the above inequality, we achieve

$$\|q_h\|_{h,D} = \left(\sum_{e \in \mathcal{E}_h^D} h_e \|q_h\|_{0,e}^2 \right)^{1/2} \leq \left(\sum_{K \in \mathcal{T}_h} h_K \|q_h\|_{0,\partial K}^2 \right)^{1/2} \leq C_{\mathrm{tr}} \left(\sum_{K \in \mathcal{T}_h} \|q_h\|_{0,K}^2 \right)^{1/2} = C_{\mathrm{tr}} \|q_h\|_{0,\Omega}.$$

Applying again Lemmas 4.1 and 4.2 for the piecewise polynomials in vector form leads to

$$\left(\sum_{e \in \mathcal{E}_h^D} h_e \left\| \boldsymbol{\varepsilon}\left(\Pi_{K_e}^{\boldsymbol{\varepsilon},k} \boldsymbol{v}_h \right) \boldsymbol{n} \right\|_{0,e}^2 \right)^{1/2} \leq \left(\sum_{K \in \mathcal{T}_h} h_K \left\| \boldsymbol{\varepsilon}\left(\Pi_K^{\boldsymbol{\varepsilon},k} \boldsymbol{v}_h \right) \boldsymbol{n} \right\|_{0,\partial K}^2 \right)^{1/2} \leq \tilde{C}_{\mathrm{tr}} \left(\sum_{K \in \mathcal{T}_h} \left\| \boldsymbol{\varepsilon}\left(\Pi_K^{\boldsymbol{\varepsilon},k} \boldsymbol{v}_h \right) \right\|_{0,K}^2 \right)^{1/2}.$$

From definition (3.2), we have $\|\boldsymbol{\varepsilon}(\Pi_K^{\boldsymbol{\varepsilon},k} \boldsymbol{v}_h)\|_{0,K} \leq C_\Pi \|\boldsymbol{\varepsilon}(\boldsymbol{v}_h)\|_{0,K}$ for all $K \in \mathcal{T}_h$, and thus, we conclude the inequality with $C_T := \tilde{C}_{\mathrm{tr}} C_\Pi$. □

Next, we introduce the following discrete norms on boundary parts as,

$$\|\boldsymbol{v}_h\|_{1/2,h,D}^2 := \sum_{e \in \mathcal{E}_h^D} h_e^{-1} \|\boldsymbol{v}_h\|_{0,e}^2, \qquad \text{and} \qquad \|\boldsymbol{v}_h\|_{1/2,h,N}^2 := \sum_{e \in \mathcal{E}_h^N} h_e^{-1} \|\boldsymbol{v}_h \cdot \boldsymbol{n}\|_{0,e}^2.$$

Now, we have that the discrete forms satisfy the following properties.

Lemma 4.4. *The boundary terms are bounded, for all $\boldsymbol{u}_h, \boldsymbol{v}_h \in \mathbf{V}_h^k$, $q_h \in Q_h^{k-1}$, as follows:*

$$\begin{aligned}
\mathcal{N}_h^{S,D}(\boldsymbol{u}_h, \boldsymbol{v}_h) &\leq \gamma_D \|\boldsymbol{u}_h\|_{1/2,h,D} \|\boldsymbol{v}_h\|_{1/2,h,D}, \\
\mathcal{N}_h^{B,D}(\boldsymbol{u}_h, \boldsymbol{v}_h) &\leq C_T \nu \|\boldsymbol{\varepsilon}(\boldsymbol{u}_h)\|_{0,\Omega} \|\boldsymbol{v}_h\|_{1/2,h,D}, \\
\mathcal{N}_h^{b,D}(\boldsymbol{v}_h, q_h) &\leq C_{tr} \|q_h\|_{0,\Omega} \|\boldsymbol{v}_h\|_{1/2,h,D}, \\
\mathcal{N}_h^{S,N}(\boldsymbol{u}_h, \boldsymbol{v}_h) &\leq \gamma_N \|\boldsymbol{u}_h\|_{1/2,h,N} \|\boldsymbol{v}_h\|_{1/2,h,N}, \\
\mathcal{N}_h^{B,N}(\boldsymbol{u}_h, \boldsymbol{v}_h) &\leq C_T\, \nu \|\boldsymbol{\varepsilon}(\boldsymbol{u}_h)\|_{0,\Omega} \|\boldsymbol{v}_h\|_{1/2,h,N}, \\
\mathcal{N}_h^{b,N}(\boldsymbol{v}_h, q_h) &\leq C_{tr} \|q_h\|_{0,\Omega} \|\boldsymbol{v}_h\|_{1/2,h,N}.
\end{aligned}$$

Proof. We start with the first bound. The Cauchy–Schwarz inequality yields

$$\mathcal{N}_h^{S,D}(\boldsymbol{u}_h,\boldsymbol{v}_h) \leq \gamma_D \sum_{e\in\mathcal{E}_h^D}\left(\int_e h_e^{-1}\boldsymbol{u}_h^2\right)^{1/2}\left(\int_e h_e^{-1}\boldsymbol{v}_h^2\right)^{1/2} \leq \gamma_D \|\boldsymbol{u}_h\|_{1/2,h,D}\|\boldsymbol{v}_h\|_{1/2,h,D}.$$

Next, by using the Cauchy–Schwarz inequality and the use of Lemma 4.3 leads to

$$\begin{aligned}\mathcal{N}_h^{B,D}(\boldsymbol{u}_h,\boldsymbol{v}_h) &\leq \sum_{e\in\mathcal{E}_h^D} \nu h_e^{1/2}\left\|\boldsymbol{\varepsilon}\left(\Pi_{K_e}^{\boldsymbol{\varepsilon},k}\boldsymbol{u}_h\right)\boldsymbol{n}\right\|_{0,e} h_e^{-1/2}\|\boldsymbol{v}_h\|_{0,e}\\ &\leq C_T\nu\|\boldsymbol{\varepsilon}(\boldsymbol{u}_h)\|_{0,\Omega}\left(\sum_{e\in\mathcal{E}_h^D} h_e^{-1}\|\boldsymbol{v}_h\|_{0,e}^2\right)^{1/2}.\end{aligned}$$

Proceeding, in similar manner and using that $\|\boldsymbol{n}\|_{\infty,e}=1$, we get the bound

$$\mathcal{N}_h^{b,D}(\boldsymbol{v}_h,q_h) \leq \sum_{e\in\mathcal{E}_h^D} h_e^{1/2}\|q_h\|_{0,e}\|\boldsymbol{n}\|_{\infty,e}h_e^{-1/2}\|\boldsymbol{v}_h\|_{0,e} \leq C_{\mathrm{tr}}\|q_h\|_{0,\Omega}\left(\sum_{e\in\mathcal{E}_h^D} h_e^{-1}\|\boldsymbol{v}_h\|_{0,e}^2\right)^{1/2}.$$

On boundary Γ_N, we have

$$\mathcal{N}_h^{S,N}(\boldsymbol{u}_h,\boldsymbol{v}_h) \leq \gamma_N \sum_{e\in\mathcal{E}_h^N}\left(\int_e h_e^{-1}(\boldsymbol{u}_h\cdot\boldsymbol{n})^2\right)^{1/2}\left(\int_e h_e^{-1}(\boldsymbol{v}_h\cdot\boldsymbol{n})^2\right)^{1/2} \leq \gamma_N\|\boldsymbol{u}_h\|_{1/2,h,N}\|\boldsymbol{v}_h\|_{1/2,h,N}.$$

Next, as before, by using the bound of unit normal $\|\boldsymbol{n}\|_{\infty,e}=1$ and Lemma 4.3, we have

$$\mathcal{N}_h^{B,N}(\boldsymbol{u}_h,\boldsymbol{v}_h) \leq \sum_{e\in\mathcal{E}_h^N} \nu\|\boldsymbol{n}\|_{\infty,e}h_e^{1/2}\left\|\boldsymbol{\varepsilon}\left(\Pi_{K_e}^{\boldsymbol{\varepsilon},k}\boldsymbol{u}_h\right)\boldsymbol{n}\right\|_{0,e} h_e^{-1/2}\|\boldsymbol{v}_h\cdot\boldsymbol{n}\|_{0,e} \leq \nu C_T\|\boldsymbol{\varepsilon}(\boldsymbol{u}_h)\|_{0,\Omega}\|\boldsymbol{v}_h\|_{1/2,h,N}.$$

Using again the previous arguments gives

$$\mathcal{N}_h^{b,N}(\boldsymbol{v}_h,q_h) \leq \sum_{e\in\mathcal{E}_h^N} h_e^{1/2}\|q_h\|_{0,e}h_e^{-1/2}\|\boldsymbol{v}_h\cdot\boldsymbol{n}\|_{0,e} \leq C_{\mathrm{tr}}\|q_h\|_{0,\Omega}\left(\sum_{e\in\mathcal{E}_h^N} h_e^{-1}\|\boldsymbol{v}_h\cdot\boldsymbol{n}\|_{0,e}^2\right)^{1/2}.$$

Thus, the proof is complete. □

Define the mesh-dependent norm for all $\boldsymbol{v}_h \in \mathbf{V}_h^k$ as,

$$|||\boldsymbol{v}_h|||_h^2 := |||\boldsymbol{v}_h|||_{\mathbf{V}}^2 + \|\boldsymbol{v}_h\|_{1/2,h,D}^2 + \|\boldsymbol{v}_h\|_{1/2,h,N}^2,$$

and the parameter-dependent discrete norm on $\mathbb{V}_h^k$ as

$$|||(\boldsymbol{v}_h,q_h)|||_h^2 := |||\boldsymbol{v}_h|||_h^2 + \|q_h\|_{0,\Omega}^2.$$

4.1. Boundedness of the forms $\mathcal{A}_h$ and $\mathcal{L}_h$

In this subsection, we show the boundedness for the presented discrete forms in the discrete formulation. We start by bounding every term in the definitions of $\mathcal{A}_h$ and $\mathcal{L}_h$.

– $m_h(\cdot,\cdot)$ is bounded. In fact, we have that

$$\begin{aligned} m_h(\boldsymbol{u}_h,\boldsymbol{v}_h) &\leq \sum_{K\in\mathcal{T}_h} \Big(m^K\Big(\boldsymbol{\Pi}_K^{0,k}\boldsymbol{u}_h,\boldsymbol{\Pi}_K^{0,k}\boldsymbol{u}_h\Big)^{1/2} m^K\Big(\boldsymbol{\Pi}_K^{0,k}\boldsymbol{v}_h,\boldsymbol{\Pi}_K^{0,k}\boldsymbol{v}_h\Big)^{1/2} \\ &\quad + \xi_2\, m^K\Big(\Big(\mathbf{I}-\boldsymbol{\Pi}_K^{0,k}\Big)\boldsymbol{u}_h,\Big(\mathbf{I}-\boldsymbol{\Pi}_K^{0,k}\Big)\boldsymbol{u}_h\Big)^{1/2} m^K\Big(\Big(\mathbf{I}-\boldsymbol{\Pi}_K^{0,k}\Big)\boldsymbol{v}_h,\Big(\mathbf{I}-\boldsymbol{\Pi}_K^{0,k}\Big)\boldsymbol{v}_h\Big)^{1/2}\Big) \\ &\leq \max\{1,\xi_2\}\sum_{K\in\mathcal{T}_h} m^K(\boldsymbol{u}_h,\boldsymbol{u}_h)\, m^K(\boldsymbol{v}_h,\boldsymbol{v}_h) = \xi^*\Big\|\mathbb{K}^{-1/2}\boldsymbol{u}_h\Big\|_{0,\Omega}\Big\|\mathbb{K}^{-1/2}\boldsymbol{v}_h\Big\|_{0,\Omega}, \end{aligned}$$

where we have used (3.4) and with $\xi^* := \max\{1,\xi_2\}$.

– $a_h(\cdot,\cdot)$ is bounded:

$$\begin{aligned} a_h^K(\boldsymbol{u}_h,\boldsymbol{v}_h) &\leq \Big(a^K\Big(\boldsymbol{\Pi}_K^{\boldsymbol{\varepsilon},k}\boldsymbol{u}_h,\boldsymbol{\Pi}_K^{\boldsymbol{\varepsilon},k}\boldsymbol{u}_h\Big)^{1/2} a^K\Big(\boldsymbol{\Pi}_K^{\boldsymbol{\varepsilon},k}\boldsymbol{v}_h,\boldsymbol{\Pi}_K^{\mathbf{0},k}\boldsymbol{v}_h\Big)^{1/2} \\ &\quad + \zeta_2\, a^K\Big(\Big(\mathbf{I}-\boldsymbol{\Pi}_K^{\boldsymbol{\varepsilon},k}\Big)\boldsymbol{u}_h,\Big(\mathbf{I}-\boldsymbol{\Pi}_K^{\boldsymbol{\varepsilon},k}\Big)\boldsymbol{u}_h\Big)^{1/2} a^K\Big(\Big(\mathbf{I}-\boldsymbol{\Pi}_K^{\boldsymbol{\varepsilon},k}\Big)\boldsymbol{v}_h,\Big(\mathbf{I}-\boldsymbol{\Pi}_K^{\boldsymbol{\varepsilon},k}\Big)\boldsymbol{v}_h\Big)^{1/2}\Big) \\ &\leq \max\{1,\zeta_2\}\, a^K(\boldsymbol{u}_h,\boldsymbol{u}_h)\, a^K(\boldsymbol{v}_h,\boldsymbol{v}_h) = \max\{1,\zeta_2\}\,\nu\|\boldsymbol{\varepsilon}(\boldsymbol{u}_h)\|_{0,K}\|\boldsymbol{\varepsilon}(\boldsymbol{v}_h)\|_{0,K}, \end{aligned}$$

where we have used (3.4). Thus, we obtain

$$\begin{aligned} a_h(\boldsymbol{u}_h,\boldsymbol{v}_h) &:= \sum_{K\in\mathcal{T}_h} a_h(\boldsymbol{u}_h,\boldsymbol{v}_h) + \mathcal{N}_h^{S,D}(\boldsymbol{u}_h,\boldsymbol{v}_h) + \mathcal{N}_h^{B,D}(\boldsymbol{u}_h,\boldsymbol{v}_h) + \mathcal{N}_h^{B,D}(\boldsymbol{v}_h,\boldsymbol{u}_h) \\ &\quad + \mathcal{N}_h^{S,N}(\boldsymbol{u}_h,\boldsymbol{v}_h) + \mathcal{N}_h^{B,N}(\boldsymbol{u}_h,\boldsymbol{v}_h) + \mathcal{N}_h^{B,N}(\boldsymbol{v}_h,\boldsymbol{u}_h) \\ &\leq \max\{1,\zeta_2\}\,\nu\|\boldsymbol{\varepsilon}(\boldsymbol{u}_h)\|_{0,\Omega}\|\boldsymbol{\varepsilon}(\boldsymbol{v}_h)\|_{0,\Omega} + \gamma_D\|\boldsymbol{u}_h\|_{1/2,h,D}\|\boldsymbol{v}_h\|_{1/2,h,D} + C_T\nu\|\boldsymbol{\varepsilon}(\boldsymbol{u}_h)\|_{0,\Omega}\|\boldsymbol{v}_h\|_{1/2,h,D} \\ &\quad + C_T\nu\|\boldsymbol{\varepsilon}(\boldsymbol{v}_h)\|_{0,\Omega}\|\boldsymbol{u}_h\|_{1/2,h,D} + \gamma_N\|\boldsymbol{u}_h\|_{1/2,h,N}\|\boldsymbol{v}_h\|_{1/2,h,N} + C_T\,\nu\|\boldsymbol{\varepsilon}(\boldsymbol{u}_h)\|_{0,\Omega}\|\boldsymbol{v}_h\|_{1/2,h,N} \\ &\quad + C_T\,\nu\|\boldsymbol{\varepsilon}(\boldsymbol{v}_h)\|_{0,\Omega}\|\boldsymbol{u}_h\|_{1/2,h,N} \\ &\leq \zeta^*\big(\nu\|\boldsymbol{\varepsilon}(\boldsymbol{u}_h)\|_{0,\Omega}^2 + \|\boldsymbol{u}_h\|_{1/2,h,D}^2 + \|\boldsymbol{u}_h\|_{1/2,h,N}^2\big)^{1/2}\big(\nu\|\boldsymbol{\varepsilon}(\boldsymbol{v}_h)\|_{0,\Omega}^2 + \|\boldsymbol{v}_h\|_{1/2,h,D}^2 + \|\boldsymbol{v}_h\|_{1/2,h,N}^2\big)^{1/2}, \end{aligned}$$

where $\zeta^* := (2C_T\nu^{1/2} + \gamma_D + \gamma_N + \max\{1,\zeta_2\})$.

– $b_h(\cdot,\cdot)$ is bounded:

$$\begin{aligned} b_h(\boldsymbol{v}_h,q_h) &\leq \|\operatorname{div}\boldsymbol{v}_h\|_{0,\Omega}\|q_h\|_{0,\Omega} + C_{\mathrm{tr}}\|q_h\|_{0,\Omega}\big(\|\boldsymbol{v}_h\|_{1/2,h,D} + \|\boldsymbol{v}_h\|_{1/2,h,N}\big) \\ &\leq (1+C_{\mathrm{tr}})\Big(\|\operatorname{div}\boldsymbol{v}_h\|_{0,\Omega}^2 + \|\boldsymbol{v}_h\|_{1/2,h,D}^2 + \|\boldsymbol{v}_h\|_{1/2,h,N}^2\Big)^{1/2}\|q_h\|_{0,\Omega}. \end{aligned}$$

– $F_h(\cdot)$ is bounded:

$$\begin{aligned} F_h(\boldsymbol{v}_h) &\leq \|\boldsymbol{f}_h\|_{0,\Omega}\|\boldsymbol{v}_h\|_{0,\Omega} + \gamma_D\sum_{e\in\mathcal{E}_h^D}\Big\|h_e^{-1/2}\boldsymbol{g}\Big\|_{0,e}\Big\|h_e^{-1/2}\boldsymbol{v}_h\Big\|_{0,e} + \sum_{e\in\mathcal{E}_h^D}\Big\|h_e^{-1/2}\boldsymbol{g}\Big\|_{0,e}\nu\Big\|h_e^{1/2}\boldsymbol{\varepsilon}\Big(\Pi_{K_e}^{\boldsymbol{\varepsilon},k}\boldsymbol{v}_h\Big)\boldsymbol{n}\Big\|_{0,e} \\ &\leq \Big\|\mathbb{K}^{1/2}\Big\|_{\infty,\Omega}\|\boldsymbol{f}\|_{0,\Omega}\Big\|\mathbb{K}^{-1/2}\boldsymbol{v}_h\Big\|_{0,\Omega} + \gamma_D\sum_{e\in\mathcal{E}_h^D}\Big\|h_e^{-1/2}\boldsymbol{g}\Big\|_{0,e}\Big\|h_e^{-1/2}\boldsymbol{v}_h\Big\|_{0,e} \\ &\quad + \left(\sum_{e\in\mathcal{E}_h^D}\|h_e^{-1/2}\boldsymbol{g}\|_{0,e}^2\right)^{1/2}\nu C_T\|\boldsymbol{\varepsilon}(\boldsymbol{v}_h)\|_{0,\Omega} \\ &\leq C\Big(\|\boldsymbol{f}\|_{0,\Omega}^2 + (\gamma_D+\nu\,C_T)\|\boldsymbol{g}\|_{1/2,h,D}^2\Big)^{1/2}|||\boldsymbol{v}_h|||_h, \end{aligned}$$

where we have used Lemma 4.3 and the discrete norm $\|\boldsymbol{g}\|_{1/2,h,D} := \Big(\sum_{e\in\mathcal{E}_h^D} h_e^{-1}\|\boldsymbol{g}\|_{0,e}^2\Big)^{1/2}$ (see [44]).

– $G(\cdot)$ is bounded:

$$G(q_h) \leq \sum_{e\in\mathcal{E}_h^D} h_e^{-1/2}\|\boldsymbol{g}\|_{0,e}h_e^{1/2}\|q_h\|_{0,e} \leq C_{tr}\|\boldsymbol{g}\|_{1/2,h,D}\|q_h\|_{0,\Omega},$$

where we have used the discrete trace inequality.

Thus, as a consequence of the above bounds, we have that the discrete bilinear form $\mathcal{A}_h$ and the linear form $\mathcal{L}_h$ are bounded with constants independent of the mesh-size and the physical parameters.

4.2. Global inf-sup condition

First, in the following lemma, we show that the bilinear form $b_h(\cdot,\cdot)$ satisfies the inf-sup condition on $\mathbf{V}_h^k \times Q_h^{k-1}$.

Lemma 4.5. *The bilinear form $b_h(\cdot,\cdot)$ satisfies inf-sup condition on $\mathbf{V}_h^k \times Q_h^{k-1}$, that is, there exists constant $\beta > 0$ such that*

$$\sup_{(0\neq)\boldsymbol{v}_h\in\mathbf{V}_h^k} \frac{b_h(\boldsymbol{v}_h, q_h)}{|||\boldsymbol{v}_h|||_h} \geq \beta\|q_h\|_{0,\Omega} \quad \forall q_h \in Q_h^{k-1}.$$

Proof. From [45], we have that

$$\sup_{(0\neq)\boldsymbol{v}_h\in\mathbf{V}_h^k\cap\mathbf{V}} \frac{b(\boldsymbol{v}_h, q_h)}{|||\boldsymbol{v}_h|||_{\mathbf{V}}} \geq \beta\|q_h\|_{0,\Omega} \qquad \forall q_h \in Q_h^{k-1}.$$

For $\boldsymbol{v}_h \in \mathbf{V}_h^k \cap \mathbf{V}$, $|||\boldsymbol{v}_h|||_h = |||\boldsymbol{v}_h|||_{\mathbf{V}}$ and $b_h(\boldsymbol{v}_h, q_h) = b(\boldsymbol{v}_h, q_h)$ $\forall q_h \in Q_h^{k-1}$ and thus yield

$$\sup_{(0\neq)\boldsymbol{v}_h\in\mathbf{V}_h^k\cap\mathbf{V}} \frac{b_h(\boldsymbol{v}_h, q_h)}{|||\boldsymbol{v}_h|||_h} = \sup_{(0\neq)\boldsymbol{v}_h\in\mathbf{V}_h^k\cap\mathbf{V}} \frac{b(\boldsymbol{v}_h, q_h)}{|||\boldsymbol{v}_h|||_{\mathbf{V}}}.$$

Trivially, we have $\mathbf{V}_h^k \cap \mathbf{V} \subseteq \mathbf{V}_h^k$ and achieve

$$\sup_{(0\neq)\boldsymbol{v}_h\in\mathbf{V}_h^k} \frac{b_h(\boldsymbol{v}_h, q_h)}{|||\boldsymbol{v}_h|||_h} \geq \sup_{(0\neq)\boldsymbol{v}_h\in\mathbf{V}_h^k\cap\mathbf{V}} \frac{b_h(\boldsymbol{v}_h, q_h)}{|||\boldsymbol{v}_h|||_h} \geq \beta\|q_h\|_{0,\Omega} \qquad \forall q_h \in Q_h^{k-1}.$$

□

Lemma 4.6. *For $\gamma_D, \gamma_N > \frac{2\nu C_T^2}{\min\{1,\zeta_1\}}$ and for all $\boldsymbol{v}_h \in \mathbf{V}_h^k$, there holds,*

$$m_h(\boldsymbol{v}_h, \boldsymbol{v}_h) + a_h(\boldsymbol{v}_h, \boldsymbol{v}_h) \geq (\xi_* + \zeta_*)\left(\left\|\mathbb{K}^{-1/2}\boldsymbol{v}_h\right\|_{0,\Omega}^2 + \nu\|\boldsymbol{\varepsilon}(\boldsymbol{v}_h)\|_{0,\Omega}^2 + \|\boldsymbol{v}_h\|_{1/2,h,D}^2 + \|\boldsymbol{v}_h\|_{1/2,h,N}^2\right),$$

for ξ_*, ζ_* independent of h and all the physical parameters.

Proof. Use of the lower bound of $\mathcal{S}_K^0(\cdot,\cdot)$ from (3.4), and $\xi_* := \min\{1, \xi_1\}$ yield

$$m_h(\boldsymbol{v}_h, \boldsymbol{v}_h) := \sum_{K\in\mathcal{T}_h} m_h^K(\boldsymbol{v}_h, \boldsymbol{v}_h) \geq \xi_*\left\|\mathbb{K}^{-1/2}\boldsymbol{v}_h\right\|_{0,\Omega}^2.$$

From definition of the bilinear forms, the lower bound of $\mathcal{S}_K^{\boldsymbol{\varepsilon}}(\cdot,\cdot)$ in (3.4) and using Lemma 4.4 gives

$$a_h(\boldsymbol{v}_h, \boldsymbol{v}_h) := \sum_{K\in\mathcal{T}_h} a_h^K(\boldsymbol{v}_h, \boldsymbol{v}_h) + \mathcal{N}_h^{S,D}(\boldsymbol{v}_h, \boldsymbol{v}_h) + 2\mathcal{N}_h^{B,D}(\boldsymbol{v}_h, \boldsymbol{v}_h) + \mathcal{N}_h^{S,N}(\boldsymbol{v}_h, \boldsymbol{v}_h) + 2\mathcal{N}_h^{B,N}(\boldsymbol{v}_h, \boldsymbol{v}_h)$$

$$\geq \min\{1,\zeta_1\}\nu\|\boldsymbol{\varepsilon}(\boldsymbol{v}_h)\|_{0,\Omega}^2+\gamma_D\|\boldsymbol{v}_h\|_{1/2,h,D}^2+\gamma_N\|\boldsymbol{v}_h\|_{1/2,h,N}^2-2C_T\nu\|\boldsymbol{\varepsilon}(\boldsymbol{v}_h)\|_{0,\Omega}\|\boldsymbol{v}_h\|_{1/2,h,D}$$
$$-2C_T\nu\|\boldsymbol{\varepsilon}(\boldsymbol{v}_h)\|_{0,\Omega}\|\boldsymbol{v}_h\|_{1/2,h,N}.$$

Taking $C_\zeta := \min\{1,\zeta_1\}$ and using Young's inequality with $\epsilon = C_\zeta/2 > 0$, there holds

$$2C_T\nu\|\boldsymbol{\varepsilon}(\boldsymbol{v}_h)\|_{0,\Omega}\|\boldsymbol{v}_h\|_{1/2,h,D}\leq\frac{C_\zeta}{2}\nu\|\boldsymbol{\varepsilon}(\boldsymbol{v}_h)\|_{0,\Omega}^2+\frac{2\nu C_T^2}{C_\zeta}\|\boldsymbol{v}_h\|_{1/2,h,D}^2.$$

Next, we have

$$a_h(\boldsymbol{v}_h,\boldsymbol{v}_h)\geq\frac{C_\zeta}{2}\nu\|\boldsymbol{\varepsilon}(\boldsymbol{v}_h)\|_{0,\Omega}^2+\left(\gamma_D-\frac{2\nu C_T^2}{C_\zeta}\right)\|\boldsymbol{v}_h\|_{1/2,h,D}^2+\left(\gamma_N-\frac{2\nu C_T^2}{C_\zeta}\right)\|\boldsymbol{v}_h\|_{1/2,h,N}^2.$$

Choosing $\gamma_D,\gamma_N>\frac{2\nu C_T^2}{C_\zeta}$ and choosing $\zeta_*:=\min\{\frac{C_\zeta}{2},\gamma_D-\frac{2\nu C_T^2}{C_\zeta},\gamma_N-\frac{2\nu C_T^2}{C_\zeta}\}$, we get

$$a_h(\boldsymbol{v}_h,\boldsymbol{v}_h)\geq\zeta_*\Big(\nu\|\boldsymbol{\varepsilon}(\boldsymbol{v}_h)\|_{0,\Omega}^2+\|\boldsymbol{v}_h\|_{1/2,h,D}^2+\|\boldsymbol{v}_h\|_{1/2,h,N}^2\Big).$$

Thus, we can conclude this lemma. □

In the next theorem, we prove the global inf-sup condition for the discrete bilinear form $\mathcal{A}_h(\cdot,\cdot)$.

Theorem 4.7. *For $(\boldsymbol{u}_h,p_h)\in\mathbb{V}_h^k$, there exists $(\boldsymbol{v}_h,q_h)\in\mathbb{V}_h^k$ with $|||(\boldsymbol{v}_h,q_h)|||_h\leq C|||(\boldsymbol{u}_h,p_h)|||_h$ such that*

$$\mathcal{A}_h((\boldsymbol{u}_h,p_h),(\boldsymbol{v}_h,q_h))\geq C_*|||(\boldsymbol{u}_h,p_h)|||_h^2.$$

where C_* is a constant independent of the mesh-size and the physical parameters.

Proof. We will construct here $(\boldsymbol{v}_h,q_h)\in\mathbb{V}_h^k$ such that it satisfies the statement of the theorem. For ease, we split the proof in four steps.

Step 1. By definition of $\mathcal{A}_h(\cdot,\cdot)$ and Lemma 4.6, we have

$$\mathcal{A}_h((\boldsymbol{u}_h,p_h),(\boldsymbol{u}_h,p_h))=m_h(\boldsymbol{u}_h,\boldsymbol{u}_h)+a_h(\boldsymbol{u}_h,\boldsymbol{u}_h)$$
$$\geq(\xi_*+\zeta_*)\left(\left\|\mathbb{K}^{-1/2}\boldsymbol{u}_h\right\|_{0,\Omega}^2+\nu\|\boldsymbol{\varepsilon}(\boldsymbol{u}_h)\|_{0,\Omega}^2+\|\boldsymbol{u}_h\|_{1/2,h,D}^2+\|\boldsymbol{u}_h\|_{1/2,h,N}^2\right).\tag{4.1}$$

Step 2. The discrete inf-sup condition in Lemma 4.5 gives the existence of $\boldsymbol{w}_h^*\in\mathbf{V}_h^k$ such that

$$-b_h(\boldsymbol{w}_h^*,p_h)\geq\beta_*\|p_h\|_{0,\Omega}^2\quad\text{and}\quad|||\boldsymbol{w}_h^*|||_h\leq\|p_h\|_{0,\Omega}.$$

By definition of $\mathcal{A}_h(\cdot,\cdot)$ in (3.6) with test function $(\boldsymbol{w}_h^*,0)$ followed with continuity of the bilinear forms, we get

$$\mathcal{A}_h((\boldsymbol{u}_h,p_h),(\boldsymbol{w}_h^*,0))=m_h(\boldsymbol{u}_h,\boldsymbol{w}_h^*)+a_h(\boldsymbol{u}_h,\boldsymbol{w}_h^*)+b_h(\boldsymbol{w}_h^*,p_h)$$
$$\leq(\xi^*+\zeta^*)\left(\left\|\mathbb{K}^{-1}\boldsymbol{u}_h\right\|_{0,\Omega}^2+\nu\|\boldsymbol{\varepsilon}(\boldsymbol{u}_h)\|_{0,\Omega}^2+\|\boldsymbol{u}_h\|_{1/2,h,D}^2+\|\boldsymbol{u}_h\|_{1/2,h,N}^2\right)^{1/2}|||\boldsymbol{w}_h^*|||_h$$
$$-\beta_*\|p_h\|_{0,\Omega}^2$$
$$\leq(\xi^*+\zeta^*)\left(\left\|\mathbb{K}^{-1}\boldsymbol{u}_h\right\|_{0,\Omega}^2+\nu\|\boldsymbol{\varepsilon}(\boldsymbol{u}_h)\|_{0,\Omega}^2+\|\boldsymbol{u}_h\|_{1/2,h,D}^2+\|\boldsymbol{u}_h\|_{1/2,h,N}^2\right)^{1/2}\|p_h\|_{0,\Omega}$$
$$-\beta_*\|p_h\|_{0,\Omega}^2.$$

By using Young's inequality with $\epsilon_1>0$ gives

$$\mathcal{A}_h((\boldsymbol{u}_h,p_h),(\boldsymbol{w}_h^*,0))\leq\frac{\epsilon_1}{2}(\xi^*+\zeta^*)\left(\|\mathbb{K}^{-1}\boldsymbol{u}_h\|_{0,\Omega}^2+\nu\|\boldsymbol{\varepsilon}(\boldsymbol{u}_h)\|_{0,\Omega}^2+\|\boldsymbol{u}_h\|_{1/2,h,D}^2+\|\boldsymbol{u}_h\|_{1/2,h,N}^2\right)$$
$$-\left(\beta_*-\frac{1}{2\epsilon_1}(\xi^*+\zeta^*)\right)\|p_h\|_{0,\Omega}^2.\tag{4.2}$$

Step 3. Moreover, we know that for constant $c := \frac{1}{|\Omega|}\int_\Omega \operatorname{div} \boldsymbol{u}_h$, we obtain

$$\begin{aligned} b_h(\boldsymbol{u}_h, c) &= -\sum_{K\in\mathcal{T}_h} (\operatorname{div}\boldsymbol{u}_h, c)_{0,K} + \sum_{e\in\mathcal{E}_h^D} (\boldsymbol{u}_h, c\boldsymbol{n})_{0,e} + \sum_{e\in\mathcal{E}_h^N} (\boldsymbol{u}_h\cdot\boldsymbol{n}, c)_{0,e} \\ &= c\left(-\int_\Omega \operatorname{div}\boldsymbol{u}_h + \sum_{e\in\mathcal{E}_h^D\cup\mathcal{E}_h^N}\int_e (\boldsymbol{u}_h\cdot\boldsymbol{n})\,\mathrm{d}s\right) = 0 \end{aligned}$$

and $(\operatorname{div}\boldsymbol{u}_h - c) \in Q_h^{k-1}$ then, we consider

$$\begin{aligned} \mathcal{A}_h((\boldsymbol{u}_h,p_h),(\boldsymbol{0},\operatorname{div}\boldsymbol{u}_h - c)) &= -b_h(\boldsymbol{u}_h, \operatorname{div}\boldsymbol{u}_h - c) \\ &= \|\operatorname{div}\boldsymbol{u}_h\|_{0,\Omega}^2 - \sum_{e\in\mathcal{E}_h^D}(\operatorname{div}\boldsymbol{u}_h, \boldsymbol{u}_h)_{0,e} - \sum_{e\in\mathcal{E}_h^N}(\operatorname{div}\boldsymbol{u}_h, \boldsymbol{u}_h\cdot\boldsymbol{n})_{0,e} \\ &\geq \|\operatorname{div}\boldsymbol{u}_h\|_{0,\Omega}^2 - \left(\sum_{e\in\mathcal{E}_h^D\cup\mathcal{E}_h^N} h_e\|\operatorname{div}\boldsymbol{u}_h\|_{0,e}^2\right)^{1/2} \\ &\quad\times\left(\|\boldsymbol{u}_h\|_{1/2,h,D}^2 + \|\boldsymbol{u}_h\cdot\boldsymbol{n}\|_{1/2,h,N}^2\right)^{1/2}. \end{aligned}$$

Use of trace inequality in Lemma 4.3 and Young's inequality with $\epsilon_2 > 0$ gives

$$\begin{aligned} \mathcal{A}_h((\boldsymbol{u}_h,p_h),(\boldsymbol{0},\operatorname{div}\boldsymbol{u}_h - c)) &\geq \|\operatorname{div}\boldsymbol{u}_h\|_{0,\Omega}^2 - C_{\mathrm{tr}}\|\operatorname{div}\boldsymbol{u}_h\|_{0,\Omega}\left(\|\boldsymbol{u}_h\|_{1/2,h,D}^2 + \|\boldsymbol{u}_h\cdot\boldsymbol{n}\|_{1/2,h,N}^2\right)^{1/2} \\ &\geq \left(1 - \frac{\epsilon_2}{2}C_{\mathrm{tr}}\right)\|\operatorname{div}\boldsymbol{u}_h\|_{0,\Omega}^2 - \frac{C_{\mathrm{tr}}}{2\,\epsilon_2}\left(\|\boldsymbol{u}_h\|_{1/2,h,D}^2 + \|\boldsymbol{u}_h\cdot\boldsymbol{n}\|_{1/2,h,N}^2\right). \end{aligned} \tag{4.3}$$

Step 4. We employ the previous steps and consider $(\boldsymbol{v}_h, q_h) := \epsilon(\boldsymbol{u}_h, p_h) - (\boldsymbol{w}_h^*, 0) + (\boldsymbol{0}, \operatorname{div}\boldsymbol{u}_h - c)$, for some $\epsilon > 0$, and note that $(\boldsymbol{v}_h, q_h) \in \mathbb{V}_h^k$. Exploiting the bounds (4.1)–(4.3), we have

$$\begin{aligned} \mathcal{A}_h((\boldsymbol{u}_h,p_h),(\boldsymbol{v}_h,q_h)) &\geq \epsilon(\xi_* + \zeta_*)\left(\left\|\mathbb{K}^{-1/2}\boldsymbol{u}_h\right\|_{0,\Omega}^2 + \nu\|\boldsymbol{\varepsilon}(\boldsymbol{u}_h)\|_{0,\Omega}^2 + \|\boldsymbol{u}_h\|_{1/2,h,D}^2 + \|\boldsymbol{u}_h\|_{1/2,h,N}^2\right) \\ &\quad - \frac{\epsilon_1}{2}(\xi^* + \zeta^*)\left(\left\|\mathbb{K}^{-1/2}\boldsymbol{u}_h\right\|_{0,\Omega}^2 + \nu\|\boldsymbol{\varepsilon}(\boldsymbol{u}_h)\|_{0,\Omega}^2 + \|\boldsymbol{u}_h\|_{1/2,h,D}^2 + \|\boldsymbol{u}_h\|_{1/2,h,N}^2\right) \\ &\quad + \left(\beta_* - \frac{1}{2\epsilon_1}(\xi^* + \zeta^*)\right)\|p_h\|_{0,\Omega}^2 + \left(1 - \frac{\epsilon_2}{2}C_{\mathrm{tr}}\right)\|\operatorname{div}\boldsymbol{u}_h\|_{0,\Omega}^2 \\ &\quad - \frac{C_{\mathrm{tr}}}{2\,\epsilon_2}\left(\|\boldsymbol{u}_h\|_{1/2,h,D}^2 + \|\boldsymbol{u}_h\cdot\boldsymbol{n}\|_{1/2,h,N}^2\right) \\ &\geq \left(\left(\epsilon - \frac{\epsilon_1}{2}\right)(\xi_* + \zeta_*) - \frac{C_{\mathrm{tr}}}{2\,\epsilon_2}\right) \\ &\quad\times\left(\left\|\mathbb{K}^{-1/2}\boldsymbol{u}_h\right\|_{0,\Omega}^2 + \nu\|\boldsymbol{\varepsilon}(\boldsymbol{u}_h)\|_{0,\Omega}^2 + \|\boldsymbol{u}_h\|_{1/2,h,D}^2 + \|\boldsymbol{u}_h\|_{1/2,h,N}^2\right) \\ &\quad + \left(\beta_* - \frac{1}{2\epsilon_1}(\xi^* + \zeta^*)\right)\|p_h\|_{0,\Omega}^2 + \left(1 - \frac{\epsilon_2}{2}C_{\mathrm{tr}}\right)\|\operatorname{div}\boldsymbol{u}_h\|_{0,\Omega}^2. \end{aligned}$$

Taking $\epsilon := \frac{C_{\mathrm{tr}}^2 + \beta_*}{\xi_* + \zeta_*}$, $\epsilon_1 := \frac{\xi_* + \zeta_*}{\beta_*}$, and $\epsilon_2 := \frac{1}{C_{\mathrm{tr}}}$, then we obtain

$$\mathcal{A}_h((\boldsymbol{u}_h,p_h),(\boldsymbol{v}_h,q_h)) \geq \frac{C_{\mathrm{tr}}^2 + \beta_*}{2}\left(\left\|\mathbb{K}^{-1/2}\boldsymbol{u}_h\right\|_{0,\Omega}^2 + \nu\|\boldsymbol{\varepsilon}(\boldsymbol{u}_h)\|_{0,\Omega}^2 + \|\boldsymbol{u}_h\|_{1/2,h,D}^2 + \|\boldsymbol{u}_h\|_{1/2,h,N}^2\right)$$

$$
\begin{aligned}
&+\frac{1}{2}\|\operatorname{div}\boldsymbol{u}_h\|_{0,\Omega}^2+\frac{\beta_*}{2}\|p_h\|_{0,\Omega}^2\\
&\geq C_*|||(\boldsymbol{u}_h,p_h)|||_h^2,
\end{aligned}
$$

with $C_*:=\frac{1}{2}(C_{\mathrm{tr}}^2+2\beta_*+1)$.

Moreover, we see that $(\boldsymbol{v}_h,q_h)=(\epsilon\boldsymbol{u}_h-\boldsymbol{w}_h^*,\epsilon p_h+\operatorname{div}\boldsymbol{u}_h-c)$ satisfies

$$
\begin{aligned}
|||(\boldsymbol{v}_h,q_h)|||_h^2&\leq\left\|\mathbb{K}^{-1/2}(\epsilon\boldsymbol{u}_h-\boldsymbol{w}_h^*)\right\|_{0,\Omega}^2+\nu\|\boldsymbol{\varepsilon}(\epsilon\boldsymbol{u}_h-\boldsymbol{w}_h^*)\|_{0,\Omega}^2+\|\operatorname{div}(\epsilon\boldsymbol{u}_h-\boldsymbol{w}_h^*)\|_{0,\Omega}^2\\
&\quad+\sum_{e\in\mathcal{E}_h^D}h_e^{-1}\|\epsilon\boldsymbol{u}_h-\boldsymbol{w}_h^*\|_{0,e}^2+\sum_{e\in\mathcal{E}_h^N}h_e^{-1}\|(\epsilon\boldsymbol{u}_h-\boldsymbol{w}_h^*)\cdot\boldsymbol{n}_e\|_{0,e}^2+\|\epsilon p_h+\operatorname{div}\boldsymbol{u}_h-c\|_{0,\Omega}^2\\
&\leq\left(\frac{C_{\mathrm{tr}}^2+\beta_*}{\xi_*+\zeta_*}+2\right)\left(|||\boldsymbol{u}_h|||_h^2+\|p_h\|_{0,\Omega}^2\right)\leq C|||(\boldsymbol{u}_h,p_h)|||_h^2,
\end{aligned}
$$

with $C:=\left(\frac{C_{\mathrm{tr}}^2+\beta_*}{\xi_*+\zeta_*}+2\right)$. □

Now, we are in position to establish the solvability and the stability properties of the discrete problem (3.5). The proof is a direct consequence of the above results.

Theorem 4.8. *For given $\boldsymbol{f}\in[L^2(\Omega)]^2$ and $\boldsymbol{g}\in[H^{1/2}(\Gamma_D)]^2$, the discrete problem (3.6) is well-posed and the solution $(\boldsymbol{u}_h,p_h)\in\mathbb{V}_h^k$ satisfies*

$$
|||(\boldsymbol{u}_h,p_h)|||_h\leq C\Big(\|\boldsymbol{f}\|_{0,\Omega}^2+(\gamma_D+\nu\,C_T+C_{tr})\|\boldsymbol{g}\|_{1/2,h,D}^2\Big)^{1/2}.
$$

where C is a constant independent of viscosity ν and mesh size h.

5. Error analysis

We assume the regularity of the given data $\boldsymbol{f}\in[H^{\max\{0,\delta-1\}}(\Omega)]^2$ and $\boldsymbol{g}\in[H^{\delta+\frac{1}{2}}(\Gamma_D)]^2$ with $\delta>1/2$ then we have the regularity estimate for the continuous solutions as

$$
\|\boldsymbol{u}\|_{1+\delta,\Omega}+\|p\|_{\delta,\Omega}\leq C_{\mathrm{reg}}\Big(\|\boldsymbol{f}\|_{\max\{0,\delta-1\},\Omega}+\|\boldsymbol{g}\|_{\delta+\frac{1}{2},\Gamma_D}\Big).\tag{5.1}
$$

Lemma 5.1 (Polynomial approximation)**.** *For $\boldsymbol{u}\in[H^{1+\delta}(\Omega)]^2$ with $\delta>0$, there exists a polynomial approximation $\boldsymbol{u}_\pi|_K\in[\mathbb{P}_k(K)]^2$ for each polygon K and satisfies*

$$
\sum_{K\in\mathcal{T}_h}\Big(\|\boldsymbol{u}-\boldsymbol{u}_\pi\|_{0,K}+h|\boldsymbol{u}-\boldsymbol{u}_\pi|_{1,K}\Big)\lesssim h^{\min\{k,\delta\}+1}|\boldsymbol{u}|_{1+\delta,\Omega}.
$$

Lemma 5.2 (Interpolation approximation)**.** *For $\boldsymbol{u}\in[H^{1+\delta}(\Omega)]^2$ with $\delta>0$, there exists a polynomial approximation $\boldsymbol{u}_I\in\mathbf{V}_h^k$ and satisfies*

$$
\|\boldsymbol{u}-\boldsymbol{u}_I\|_{0,\Omega}+h|\boldsymbol{u}-\boldsymbol{u}_I|_{1,\Omega}\lesssim h^{\min\{k,\delta\}+1}|\boldsymbol{u}|_{1+\delta,\Omega}.
$$

The following theorem provides the rate of convergence of our virtual element scheme with Nitsche stabilization, for the Brinkman problem with mixed boundary conditions, presented in (3.5).

Theorem 5.3. *Let $(\boldsymbol{u},p)\in\mathbf{V}_g\times Q$ and $(\boldsymbol{u}_h,p_h)\in\mathbf{V}_h^k\times Q_h^{k-1}$ be the solutions of the continuous and discrete problems. Assuming $\boldsymbol{f}\in[H^{\max\{\delta,k\}-1}(\Omega)]^2$ and $\boldsymbol{g}\in[H^{\delta+\frac{1}{2}}(\Gamma_D)]^2$ for $\delta>1/2$, there holds*

$$
|||(\boldsymbol{u},p)-(\boldsymbol{u}_h,p_h)|||_h\leq Ch^{\min\{\delta,k\}}\Big(\|\boldsymbol{f}\|_{\max\{\delta,k\}-1,\Omega}+\|\boldsymbol{g}\|_{\delta+\frac{1}{2},\Gamma_D}\Big),
$$

where C is a generic constant independent of ν and h.

Proof. Let $\boldsymbol{\rho}_h := (\boldsymbol{u}_h, p_h) - (\boldsymbol{v}_h, q_h) \in \mathbb{V}_h^k$. Then, as a consequence of the global inf-sup condition in Theorem 4.7, we have

$$
\begin{aligned}
C|||\boldsymbol{\rho}_h|||_h &\leq \sup_{((\mathbf{0},0)\neq)(\boldsymbol{w}_h,r_h)\in\mathbb{V}_h^k} \frac{\mathcal{A}_h(\boldsymbol{\rho}_h,(\boldsymbol{w}_h,r_h))}{|||(\boldsymbol{w}_h,r_h)|||_h} \\
&= \sup_{((\mathbf{0},0)\neq)(\boldsymbol{w}_h,r_h)\in\mathbb{V}_h^k} \left(\frac{\mathcal{L}_h(\boldsymbol{w}_h,r_h) - \mathcal{A}((\boldsymbol{u},p),(\boldsymbol{w}_h,r_h))}{|||(\boldsymbol{w}_h,r_h)|||_h} + \frac{\mathcal{A}((\boldsymbol{u},p),(\boldsymbol{w}_h,r_h)) - \mathcal{A}_h((\boldsymbol{v}_h,q_h),(\boldsymbol{w}_h,r_h))}{|||(\boldsymbol{w}_h,r_h)|||_h} \right).
\end{aligned}
$$

We start the error analysis by estimating the consistency error for any $(\boldsymbol{w}_h, r_h) \in \mathbf{V}_h^k \times Q_h^{k-1}$,

$$
E_c := \mathcal{L}_h((\boldsymbol{w}_h,r_h)) - \mathcal{A}((\boldsymbol{u},p),(\boldsymbol{w}_h,r_h)).
$$

Using integration by parts and the boundary conditions, we have

$$
\begin{aligned}
\mathcal{A}((\boldsymbol{u},p),(\boldsymbol{w}_h,r_h)) &= F(\boldsymbol{w}_h) + \int_{\partial\Omega} (\nu\boldsymbol{\varepsilon}(\boldsymbol{u}) - p\mathbb{I})\boldsymbol{n}\cdot\boldsymbol{w}_h \\
&= F(\boldsymbol{w}_h) + \int_{\Gamma_N} \big(\boldsymbol{n}^t(\nu\boldsymbol{\varepsilon}(\boldsymbol{u})\boldsymbol{n})(\boldsymbol{w}_h\cdot\boldsymbol{n}) + \boldsymbol{t}^t(\nu\boldsymbol{\varepsilon}(\boldsymbol{u})\boldsymbol{n})(\boldsymbol{w}_h\cdot\boldsymbol{t}) - p(\boldsymbol{w}_h\cdot\boldsymbol{n})\big) \\
&\quad + \int_{\Gamma_D} (\nu\boldsymbol{\varepsilon}(\boldsymbol{u}) - p\mathbb{I})\boldsymbol{n}\cdot\boldsymbol{w}_h \\
&= F(\boldsymbol{w}_h) + \int_{\Gamma_N} \big(\boldsymbol{n}^t(\nu\boldsymbol{\varepsilon}(\boldsymbol{u})\boldsymbol{n})(\boldsymbol{w}_h\cdot\boldsymbol{n}) - p(\boldsymbol{w}_h\cdot\boldsymbol{n})\big) + \int_{\Gamma_D} (\nu\boldsymbol{\varepsilon}(\boldsymbol{u}) - p\mathbb{I})\boldsymbol{n}\cdot\boldsymbol{w}_h.
\end{aligned}
$$

The boundary conditions (2.3) and (2.4) for continuous solution $\boldsymbol{u}$ and the continuous formulation (2.5) implies

$$
\begin{aligned}
E_c = (\langle \boldsymbol{f}_h, \boldsymbol{w}_h\rangle - (\boldsymbol{f},\boldsymbol{w}_h)) &- \left(\sum_{e\in\mathcal{E}_h^D} \int_e (\nu\boldsymbol{\varepsilon}(\boldsymbol{u}) - p\mathbb{I})\boldsymbol{n}\cdot\boldsymbol{w}_h \,\mathrm{d}s + \sum_{e\in\mathcal{E}_h^N} \int_e \big(\boldsymbol{n}^t(\nu\boldsymbol{\varepsilon}(\boldsymbol{u}) - p\mathbb{I})\boldsymbol{n}\big)(\boldsymbol{w}_h\cdot\boldsymbol{n})\,\mathrm{d}s \right) \\
+ \gamma_D \sum_{e\in\mathcal{E}_h^D} \int_e h_e^{-1}\boldsymbol{g}\cdot\boldsymbol{w}_h \,\mathrm{d}s &- \sum_{e\in\mathcal{E}_h^D} \int_e \boldsymbol{g}\cdot\Big(\nu\boldsymbol{\varepsilon}\Big(\Pi_{K_e}^{\boldsymbol{\varepsilon},k}\boldsymbol{w}_h\Big)\boldsymbol{n}\Big)\,\mathrm{d}s - \sum_{e\in\mathcal{E}_h^D} \int_e \boldsymbol{g}\cdot(r_h\boldsymbol{n})\,\mathrm{d}s.
\end{aligned}
$$

Next we use the following notation for the rest of error term as

$$
E_A := \mathcal{A}((\boldsymbol{u},p),(\boldsymbol{w}_h,r_h)) - \mathcal{A}_h((\boldsymbol{v}_h,q_h),(\boldsymbol{w}_h,r_h)).
$$

Use of continuous and discrete formulation, and polynomial approximation u_π leads to

$$
\begin{aligned}
E_A &= (m(\boldsymbol{u},\boldsymbol{w}_h) - m_h(\boldsymbol{v}_h,\boldsymbol{w}_h)) + (a(\boldsymbol{u},\boldsymbol{w}_h) - a_h(\boldsymbol{v}_h,\boldsymbol{w}_h)) + (b(\boldsymbol{w}_h,p) - b_h(\boldsymbol{w}_h,q_h)) \\
&\quad - (b(\boldsymbol{u},r_h) - b_h(\boldsymbol{v}_h,r_h)) \\
&= (m(\boldsymbol{u},\boldsymbol{w}_h) - m_h(\boldsymbol{v}_h,\boldsymbol{w}_h)) + \sum_{K\in\mathcal{T}_h} \big(a^K(\boldsymbol{u}-\boldsymbol{u}_\pi,\boldsymbol{w}_h) - a_h^K(\boldsymbol{v}_h-\boldsymbol{u}_\pi,\boldsymbol{w}_h)\big) \\
&\quad + \Big((\operatorname{div}\boldsymbol{w}_h, p-q_h)_{0,\Omega} - (\operatorname{div}(\boldsymbol{u}-\boldsymbol{v}_h), r_h)_{0,\Omega}\Big) - \Big(\mathcal{N}_h^{S,D}(\boldsymbol{v}_h,\boldsymbol{w}_h) \\
&\quad + \mathcal{N}_h^{B,D}(\boldsymbol{v}_h,\boldsymbol{w}_h) + \mathcal{N}_h^{B,D}(\boldsymbol{w}_h,\boldsymbol{v}_h) + \mathcal{N}_h^{S,N}(\boldsymbol{v}_h,\boldsymbol{w}_h) + \mathcal{N}_h^{B,N}(\boldsymbol{v}_h,\boldsymbol{w}_h) + \mathcal{N}_h^{B,N}(\boldsymbol{w}_h,\boldsymbol{v}_h)\Big) \\
&\quad - \Big(\mathcal{N}_h^{b,D}(\boldsymbol{w}_h,q_h) + \mathcal{N}_h^{b,N}(\boldsymbol{w}_h,q_h)\Big) - \Big(\mathcal{N}_h^{b,D}(\boldsymbol{v}_h,r_h) + \mathcal{N}_h^{b,N}(\boldsymbol{v}_h,r_h)\Big).
\end{aligned}
$$

Consider $E_c + E_A$ with the definition of Nitsche stabilization terms and the boundary conditions, we get

$$
E_c + E_A = (\langle \boldsymbol{f}_h, \boldsymbol{w}_h\rangle - (\boldsymbol{f},\boldsymbol{w}_h)) + (m(\boldsymbol{u},\boldsymbol{w}_h) - m_h(\boldsymbol{v}_h,\boldsymbol{w}_h)) + \sum_{K\in\mathcal{T}_h} \Big(a^K(\boldsymbol{u}-\boldsymbol{u}_\pi,\boldsymbol{w}_h) - a_h^K(\boldsymbol{v}_h-\boldsymbol{u}_\pi,\boldsymbol{w}_h)\Big)
$$

$$
\begin{aligned}
&- \Bigg(\sum_{e\in\mathcal{E}_h^D} \int_e \Big(\nu\boldsymbol{\varepsilon}\Big(\boldsymbol{u} - \Pi_K^{\boldsymbol{\varepsilon},k}\boldsymbol{v}_h\Big) - (p-q_h)\mathbb{I}\Big)\boldsymbol{n}\cdot\boldsymbol{w}_h \,\mathrm{d}s \\
&+ \sum_{e\in\mathcal{E}_h^N} \int_e \Big(\boldsymbol{n}^t\Big(\nu\boldsymbol{\varepsilon}\Big(\boldsymbol{u} - \Pi_K^{\boldsymbol{\varepsilon},k}\boldsymbol{v}_h\Big) - (p-q_h)\mathbb{I}\Big)\boldsymbol{n}\Big)(\boldsymbol{w}_h\cdot\boldsymbol{n})\,\mathrm{d}s\Bigg) + \Big((\operatorname{div}\boldsymbol{w}_h, p-q_h)_{0,\Omega} - (\operatorname{div}(\boldsymbol{u}-\boldsymbol{v}_h), r_h)_{0,\Omega}\Big) \\
&+ \gamma_D \sum_{e\in\mathcal{E}_h^D} \int_e h_e^{-1}(\boldsymbol{g}-\boldsymbol{v}_h)\cdot\boldsymbol{w}_h \,\mathrm{d}s - \sum_{e\in\mathcal{E}_h^D} \int_e (\boldsymbol{g}-\boldsymbol{v}_h)\cdot\Big(\nu\boldsymbol{\varepsilon}\Big(\Pi_{K_e}^{\boldsymbol{\varepsilon},k}\boldsymbol{w}_h\Big)\boldsymbol{n}\Big)\,\mathrm{d}s - \sum_{e\in\mathcal{E}_h^D} \int_e (\boldsymbol{g}-\boldsymbol{v}_h)\cdot(r_h\boldsymbol{n})\,\mathrm{d}s \\
&+ \gamma_N \sum_{e\in\mathcal{E}_h^N} \int_e h_e^{-1}(\boldsymbol{u}-\boldsymbol{v}_h)\cdot\boldsymbol{n}(\boldsymbol{w}_h\cdot\boldsymbol{n})\,\mathrm{d}s - \sum_{e\in\mathcal{E}_h^N} \int_e (\boldsymbol{n}^t\Big(\nu\boldsymbol{\varepsilon}\Big(\Pi_K^{\boldsymbol{\varepsilon},k}\boldsymbol{w}_h\Big)\boldsymbol{n}\Big)((\boldsymbol{u}-\boldsymbol{v}_h)\cdot\boldsymbol{n})\,\mathrm{d}s \\
&+ \sum_{e\in\mathcal{E}_h^N} \int_e r_h(\boldsymbol{u}-\boldsymbol{v}_h)\cdot\boldsymbol{n}\,\mathrm{d}s \\
&= \underbrace{(\langle\boldsymbol{f}_h,\boldsymbol{w}_h\rangle - (\boldsymbol{f},\boldsymbol{w}_h))}_{T_1} + \underbrace{(m(\boldsymbol{u},\boldsymbol{w}_h) - m_h(\boldsymbol{v}_h,\boldsymbol{w}_h))}_{T_2} + \underbrace{\sum_{K\in\mathcal{T}_h}\Big(a^K(\boldsymbol{u}-\boldsymbol{u}_\pi,\boldsymbol{w}_h) - a_h^K(\boldsymbol{v}_h-\boldsymbol{u}_\pi,\boldsymbol{w}_h)\Big)}_{T_3} \\
&+ \underbrace{\sum_{e\in\mathcal{E}_h^D} \int_e \Big(-\nu\boldsymbol{\varepsilon}\Big(\boldsymbol{u} - \Pi_K^{\boldsymbol{\varepsilon},k}\boldsymbol{v}_h\Big)\Big)\boldsymbol{n}\cdot\boldsymbol{w}_h \,\mathrm{d}s}_{T_4} + \underbrace{\sum_{e\in\mathcal{E}_h^N} \int_e \Big(-\boldsymbol{n}^t\Big(\nu\boldsymbol{\varepsilon}\Big(\boldsymbol{u} - \Pi_K^{\boldsymbol{\varepsilon},k}\boldsymbol{v}_h\Big)\Big)\boldsymbol{n}\Big)(\boldsymbol{w}_h\cdot\boldsymbol{n})\,\mathrm{d}s}_{T_5} \\
&+ \underbrace{\sum_{e\in\mathcal{E}_h^D} \int_e \Big((\gamma_D h_e^{-1}(\boldsymbol{g}-\boldsymbol{v}_h)\cdot\boldsymbol{w}_h) - \Big((\boldsymbol{g}-\boldsymbol{v}_h)\cdot\Big(\nu\boldsymbol{\varepsilon}\Big(\Pi_{K_e}^{\boldsymbol{\varepsilon},k}\boldsymbol{w}_h\Big)\boldsymbol{n}\Big)\Big) - ((\boldsymbol{g}-\boldsymbol{v}_h)\cdot(r_h\boldsymbol{n}))\Big)\,\mathrm{d}s}_{T_6} \\
&+ \underbrace{\sum_{e\in\mathcal{E}_h^N} \int_e \Big((\gamma_N h_e^{-1}(\boldsymbol{u}-\boldsymbol{v}_h)\cdot\boldsymbol{n}(\boldsymbol{w}_h\cdot\boldsymbol{n})) - \Big(\Big(\boldsymbol{n}^t\Big(\nu\boldsymbol{\varepsilon}(\Pi_K^{\boldsymbol{\varepsilon},k}\boldsymbol{w}_h)\Big)((\boldsymbol{u}-\boldsymbol{v}_h)\cdot\boldsymbol{n})\Big) + (r_h(\boldsymbol{u}-\boldsymbol{v}_h)\cdot\boldsymbol{n})\Big)\,\mathrm{d}s}_{T_7} \\
&+ \underbrace{(-b_h(\boldsymbol{w}_h,p-q_h) - (\operatorname{div}(\boldsymbol{u}-\boldsymbol{v}_h),r_h)_{0,\Omega})}_{T_8}.
\end{aligned}
$$

The Cauchy–Schwarz inequality with $C_{\mathbb{K}}$ is a constant depending on the bound $\|\mathbb{K}\|_{\infty,\Omega}$ gives

$$
\begin{aligned}
T_1 &\le C_{\mathbb{K}}\Bigg(\sum_{K\in\mathcal{T}_h}\Big\|\Big(I-\Pi_K^{0,k-1}\Big)\boldsymbol{f}\Big\|_{0,K}^2\Bigg)^{1/2}\Big\|\mathbb{K}^{-1/2}\boldsymbol{w}_h\Big\|_{0,\Omega} \\
&\le C_{\mathbb{K}}h^k|\boldsymbol{f}|_{k-1,\Omega}\Big\|\mathbb{K}^{-1/2}\boldsymbol{w}_h\Big\|_{0,\Omega}.
\end{aligned}
$$

Following [40], we can estimate T_2 as

$$
\begin{aligned}
T_2 &= \sum_{K\in\mathcal{T}_h}\Big(\Big(m^K(\boldsymbol{u},\boldsymbol{w}_h) - m_h^K(\boldsymbol{u},\boldsymbol{w}_h)\Big) + m_h^K(\boldsymbol{u}-\boldsymbol{v}_h,\boldsymbol{w}_h)\Big) \\
&= \sum_{K\in\mathcal{T}_h}\Big((\mathbb{K}^{-1}\boldsymbol{u},\boldsymbol{w}_h)_{0,K} - \Big(\mathbb{K}^{-1}\Pi_K^{0,k}\boldsymbol{u},\Pi_K^{0,k}\boldsymbol{w}_h\Big)_{0,K} - S_K^0\Big(\Big(\mathbf{I}-\Pi_K^{0,k}\Big)\boldsymbol{u},\Big(\mathbf{I}-\Pi_K^{0,k}\Big)\boldsymbol{w}_h\Big) + m_h^K(\boldsymbol{u}-\boldsymbol{v}_h,\boldsymbol{w}_h)\Big) \\
&= \sum_{K\in\mathcal{T}_h}\Big(\Big(\Big(\mathbf{I}-\Pi_K^{0,k}\Big)(\mathbb{K}^{-1}\boldsymbol{u}),\Big(\mathbf{I}-\Pi_K^{0,k}\Big)\boldsymbol{w}_h\Big)_{0,K} - \Big(\Big(\mathbf{I}-\Pi_K^{0,k}\Big)\boldsymbol{u},\Big(\mathbf{I}-\Pi_K^{0,k}\Big)(\mathbb{K}^{-1}\boldsymbol{w}_h)\Big)_{0,K} \\
&\quad + \Big(\Big(\mathbf{I}-\Pi_K^{0,k}\Big)\boldsymbol{u},\mathbb{K}^{-1}\Big(\mathbf{I}-\Pi_K^{0,k}\Big)\boldsymbol{w}_h\Big)_{0,K} - S_K^0\Big(\Big(\mathbf{I}-\Pi_K^{0,k}\Big)\boldsymbol{u},\Big(\mathbf{I}-\Pi_K^{0,k}\Big)\boldsymbol{w}_h\Big) + m_h^K(\boldsymbol{u}-\boldsymbol{v}_h,\boldsymbol{w}_h)\Big)
\end{aligned}
$$

$$\leq C_{\mathbb{K}} \sum_{K\in\mathcal{T}_h} \Big(\Big\| \Big(\mathbf{I}-\Pi_K^{0,k}\Big)\Big(\mathbb{K}^{-1/2}\boldsymbol{u}\Big)\Big\|_{0,K} \Big\| \Big(\mathbf{I}-\Pi_K^{0,k}\Big)\Big(\mathbb{K}^{-1/2}\boldsymbol{w}_h\Big)\Big\|_{0,K}$$
$$+ \|\mathbb{K}^{-1}\|_{\infty,K} \Big\| \Big(\mathbf{I}-\Pi_K^{0,k}\Big)\boldsymbol{u}\Big\|_{0,K} \Big\| \Big(\mathbf{I}-\Pi_K^{0,k}\Big)\boldsymbol{w}_h\Big\|_{0,K} + \|\boldsymbol{u}-\boldsymbol{v}_h\|_{0,K} \Big\|\mathbb{K}^{-1/2}\boldsymbol{w}_h\Big\|_{0,K}\Big)$$
$$\leq C_{\mathbb{K}} \left(h^{\min\{\delta,k\}} |\boldsymbol{u}|_{1+\delta,\Omega} + \left(\sum_{K\in\mathcal{T}_h} \|\boldsymbol{u}-\boldsymbol{v}_h\|_{0,K}^2 \right)^{1/2} \right) \|\mathbb{K}^{-1/2}\boldsymbol{w}_h\|_{0,\Omega}.$$

Use of polynomial approximation in Lemma 5.1, polynomial consistency and continuity of the discrete bilinear form $a_h(\cdot,\cdot)$ leads to

$$T_3 = \sum_{K\in\mathcal{T}_h} \left(a^K(\boldsymbol{u}-\boldsymbol{u}_\pi,\boldsymbol{w}_h) - a_h^K(\boldsymbol{v}_h-\boldsymbol{u}_\pi,\boldsymbol{w}_h)\right)$$
$$\leq 2 \left(\sum_{K\in\mathcal{T}_h} \nu \Big(\|\boldsymbol{\varepsilon}(\boldsymbol{u}-\boldsymbol{u}_\pi)\|_{0,K}^2 + \|\boldsymbol{\varepsilon}(\boldsymbol{u}-\boldsymbol{v}_h)\|_{0,K}^2 \Big) \right)^{1/2} \left(\sum_{K\in\mathcal{T}_h} \nu \|\boldsymbol{\varepsilon}(\boldsymbol{w}_h)\|_{0,K}^2 \right)^{1/2}$$
$$\lesssim \left(h^{\min\{\delta,k\}} |\boldsymbol{u}|_{1+\delta,\Omega} + \left(\sum_{K\in\mathcal{T}_h} \|\boldsymbol{u}-\boldsymbol{v}_h\|_{0,K}^2 \right)^{1/2} \right) \nu \|\boldsymbol{\varepsilon}(\boldsymbol{w}_h)\|_{0,\Omega}.$$

Combination of Cauchy–Schwarz inequality and Lemma 4.3 gives

$$T_4 \leq \sum_{e\in\mathcal{E}_h^D} h_e^{1/2} \Big\| \nu\boldsymbol{\varepsilon}\Big(\Big(\mathbf{I}-\Pi_{K_e}^{\boldsymbol{\varepsilon},k}\Big)\boldsymbol{u}\Big)\boldsymbol{n}\Big\|_{0,e} h_e^{-1/2} \|\boldsymbol{w}_h\|_{0,e}$$
$$\leq \nu C_T \left(\sum_{K\in\mathcal{T}_h} \Big\| \boldsymbol{\varepsilon}\Big(\Big(\mathbf{I}-\Pi_K^{\boldsymbol{\varepsilon},k}\Big)\boldsymbol{u}\Big)\Big\|_{0,K}^2 \right)^{1/2} \|\boldsymbol{w}_h\|_{1/2,h,D}$$
$$\lesssim \nu C_T\, h^{\min\{\delta,k\}}\, |\boldsymbol{u}|_{1+\delta,\Omega} \|\boldsymbol{w}_h\|_{1/2,h,D}.$$

In similar manner as the bound for term T_4, there holds

$$T_5 \leq \sum_{e\in\mathcal{E}_h^N} h_e^{1/2} \Big\| \nu\boldsymbol{\varepsilon}\Big(\Big(\mathbf{I}-\Pi_{K_e}^{\boldsymbol{\varepsilon},k}\Big)\boldsymbol{u}\Big)\boldsymbol{n}\Big\|_{0,e} h_e^{-1/2} \|\boldsymbol{w}_h\cdot\boldsymbol{n}\|_{0,e}$$
$$\leq \nu C_T \left(\sum_{K\in\mathcal{T}_h} \Big\| \boldsymbol{\varepsilon}\Big(\Big(\mathbf{I}-\Pi_{K_e}^{\boldsymbol{\varepsilon},k}\Big)\boldsymbol{u}\Big)\Big\|_{0,K_e}^2 \right)^{1/2} \|\boldsymbol{w}_h\|_{1/2,h,N}$$
$$\lesssim \nu\, C_T\, h^{\min\{\delta,k\}} |\boldsymbol{u}|_{1+\delta,\Omega} \|\boldsymbol{w}_h\|_{1/2,h,N}.$$

Use of trace inequality leads to

$$T_6 = \sum_{e\in\mathcal{E}_h^D} \int_e \Big(\big(\gamma_D h_e^{-1}(\boldsymbol{g}-\boldsymbol{v}_h)\cdot\boldsymbol{w}_h\big) - \Big((\boldsymbol{g}-\boldsymbol{v}_h)\cdot\Big(\nu\boldsymbol{\varepsilon}\Big(\Pi_{K_e}^{\boldsymbol{\varepsilon},k}\boldsymbol{w}_h\Big)\boldsymbol{n}\Big)\Big) - ((\boldsymbol{g}-\boldsymbol{v}_h)\cdot(r_h\boldsymbol{n}))\Big)\,\mathrm{d}s$$
$$\leq \sum_{e\in\mathcal{E}_h^D} \Big(h_e^{-1/2}\|\boldsymbol{u}-\boldsymbol{v}_h\|_{0,e}\Big) \Big(\gamma_D h_e^{-1/2}\|\boldsymbol{w}_h\|_{0,e} + \nu h_e^{1/2} \Big\|\boldsymbol{\varepsilon}\Big(\Pi_{K_e}^{\boldsymbol{\varepsilon},k}\boldsymbol{w}_h\Big)\boldsymbol{n}\Big\|_{0,e} + h_e^{1/2}\|r_h\|_{0,e}\Big)$$
$$\leq C_t \sum_{K\in\mathcal{T}_h} \Big(h_K^{-1}\|\boldsymbol{u}-\boldsymbol{v}_h\|_{0,K} + |\boldsymbol{u}-\boldsymbol{v}_h|_{1,K}\Big) \Big(\gamma_D\|\boldsymbol{w}_h\|_{1/2,h,D} + \nu C_T\|\boldsymbol{w}_h\|_{0,\Omega} + C_{\mathrm{tr}}\|r_h\|_{0,\Omega}\Big).$$

For Neumann condition, we use the same results and obtain

$$\begin{aligned}
T_7 &= \sum_{e\in\mathcal{E}_h^N}\int_e \Big(\big(\gamma_N h_e^{-1}(\boldsymbol{u}-\boldsymbol{v}_h)\cdot\boldsymbol{n}(\boldsymbol{w}_h\cdot\boldsymbol{n})\big) - \Big(\Big(\boldsymbol{n}^t\Big(\nu\boldsymbol{\varepsilon}\Big(\Pi_K^{\boldsymbol{\varepsilon},k}\boldsymbol{w}_h\Big)\Big)((\boldsymbol{u}-\boldsymbol{v}_h)\cdot\boldsymbol{n})\Big) + (r_h(\boldsymbol{u}-\boldsymbol{v}_h)\cdot\boldsymbol{n})\Big)\,\mathrm{d}s\\
&\le \sum_{e\in\mathcal{E}_h^N}\Big(h_e^{-1/2}\|\boldsymbol{u}-\boldsymbol{v}_h\|_{0,e}\Big)\Big(\gamma_N h_e^{-1/2}\|\boldsymbol{w}_h\cdot\boldsymbol{n}\|_{0,e} + \nu h_e^{1/2}\Big\|\boldsymbol{\varepsilon}\Big(\Pi_{K_e}^{\boldsymbol{\varepsilon},k}\boldsymbol{w}_h\Big)\boldsymbol{n}\Big\|_{0,e} + h_e^{1/2}\|r_h\|_{0,e}\Big)\\
&\le C_t\sum_{K\in\mathcal{T}_h}\Big(h_K^{-1}\|\boldsymbol{u}-\boldsymbol{v}_h\|_{0,K} + |\boldsymbol{u}-\boldsymbol{v}_h|_{1,K}\Big)\Big(\gamma_N\|\boldsymbol{w}_h\|_{1/2,h,N} + \nu C_T\|\boldsymbol{w}_h\|_{0,\Omega} + C_{\mathrm{tr}}\|r_h\|_{0,\Omega}\Big).
\end{aligned}$$

Use of Lemma 4.1 with $\delta\in(1/2,1]$ leads to

$$\begin{aligned}
T_8 &= \sum_{e\in\mathcal{E}_h^N} -b_h(\boldsymbol{w}_h,p-q_h) - (\mathrm{div}(\boldsymbol{u}-\boldsymbol{v}_h),r_h)_{0,\Omega}\\
&\le \sum_{e\in\mathcal{E}_h^N} h_e^{-1/2}\|\boldsymbol{w}_h\cdot\boldsymbol{n}\|_{0,e}h_e^{1/2}\|p-q_h\|_{0,e} + \sum_{e\in\mathcal{E}_h^D} h_e^{-1/2}\|\boldsymbol{w}_h\|_{0,e}h_e^{1/2}\|p-q_h\|_{0,e}\\
&\quad + \|\mathrm{div}\,\boldsymbol{w}_h\|_{0,\Omega}\|p-q_h\|_{0,\Omega} + \|\mathrm{div}(\boldsymbol{u}-\boldsymbol{v}_h)\|_{0,\Omega}\|r_h\|_{0,\Omega}\\
&\le \Big(\|\boldsymbol{w}_h\|_{1/2,h,N} + \|\boldsymbol{w}_h\|_{1/2,h,D}\Big)\sum_{K\in\mathcal{T}_h}\big(\|p-q_h\|_{0,K} + h_K^{\delta}|p-q_h|_{\delta,K}\big)\\
&\quad + \|\mathrm{div}\,\boldsymbol{w}_h\|_{0,\Omega}\|p-q_h\|_{0,\Omega} + \|\mathrm{div}(\boldsymbol{u}-\boldsymbol{v}_h)\|_{0,\Omega}\|r_h\|_{0,\Omega}.
\end{aligned}$$

For $(\boldsymbol{v}_h,q_h) := (\boldsymbol{u}_I,\Pi^{0,k-1}p)\in\mathbb{V}_h^k$ with $\Pi^{0,k-1}p|_K := \Pi_K^{0,k-1}p$ for all $K\in\mathcal{T}_h$ in the term T_1–T_8 to achieve

$$|||\boldsymbol{\rho}_h|||_h \le |||(\boldsymbol{u},p)-\big(\boldsymbol{u}_I,\Pi^{0,k-1}p\big)|||_h + Ch^{\min\{k,\delta\}}\big(|\boldsymbol{f}|_{\max\{\delta,k\}-1,\Omega} + |\boldsymbol{u}|_{1+\delta,\Omega} + |p|_{\delta,\Omega}\big).$$

The triangle inequality along with the previous bound for $|||\boldsymbol{\rho}_h|||_h$ yield

$$\begin{aligned}
|||(\boldsymbol{u},p)-(\boldsymbol{u}_h,p_h)|||_h &\le |||(\boldsymbol{u},p)-\big(\boldsymbol{u}_I,\Pi^{0,k-1}p\big)|||_h + |||\big(\boldsymbol{u}_I,\Pi^{0,k-1}p\big)-(\boldsymbol{u}_h,p_h)|||_h\\
&\le 2|||(\boldsymbol{u},p)-\big(\boldsymbol{u}_I,\Pi^{0,k-1}p\big)|||_h + C\,h^{\min\{k,\delta\}}\big(|\boldsymbol{f}|_{\max\{\delta,k\}-1,\Omega} + |\boldsymbol{u}|_{1+\delta,\Omega} + |p|_{\delta,\Omega}\big).
\end{aligned}$$

Lemma 5.2 and regularity estimate (5.1) conclude

$$\begin{aligned}
|||(\boldsymbol{u},p)-(\boldsymbol{u}_h,p_h)|||_h &\lesssim h^{\min\{k,\delta\}}\Big(|\boldsymbol{f}|_{\max\{\delta,k\}-1,\Omega} + |\boldsymbol{u}|_{1+\delta,\Omega} + |p|_{\delta,\Omega}\Big)\\
&\le Ch^{\min\{\delta,k\}}\Big(\|\boldsymbol{f}\|_{\max\{\delta,k\}-1,\Omega} + \|\boldsymbol{g}\|_{\delta+\frac{1}{2},\Gamma_D}\Big),
\end{aligned}$$

where C is independent of physical parameter ν and mesh-size h. □

Remark 5.4. The global inf-sup condition for the continuous Taylor–Hood virtual element spaces [47] cannot be followed in the same manner due to the fact that $\mathrm{div}\,\mathbf{V}_h^k$ is a piecewise discontinuous polynomial space of degree $k-1$ while Q_h^{k-1} is continuous polynomial space of degree $k-1$, and hence the error analysis for these spaces does not follow from the previous theorem and requires a different treatment though the coercivity on the kernel of $b_h(\cdot,\cdot)$.

6. Numerical results

This section is devoted to explore different numerical experiments to verify the performance and robustness of the proposed method. The numerical approach involves the utilization of the DUNE–FEM library [26], specifically the DUNE–VEM module [25] for generating the computational spaces $\mathbf{V}_h^k$ and Q_h^{k-1}. We resort to

the DUNE–VEM tuple `DivfreeSpace` + $\mathbb{P}_0$ on polygonal meshes to construct these spaces (see [25], Sect. 3.4.3). Then, similar to [9], a more accurate pressure is recovered by an element-wise post-processing procedure. For completeness, we represent the pressure surface plots using the $\mathbb{P}_0$ discrete approximation.

In order to tackle the resulting sparse linear system $\boldsymbol{Ax} = \boldsymbol{F}$, arising from the discretization process, we employ the sparse linear solver `spsolve` from the Scipy library [46] with UMFPACK . A critical parameter in our simulations is the Nitsche parameter, which is chosen to satisfy $\gamma_D = \gamma_N = \gamma$, with $\gamma \geq 100(k+1)^2$, where k represents the order of the numerical scheme employed. This choice is inspired in [14] and guaranteed the coercivity of $a_h(\cdot,\cdot)$, and consequently the inf-sup stability of $\mathcal{A}_h((\cdot,\cdot),(\cdot,\cdot))$ in all the cases. Choosing a sharp (minimum) parameter that maintains stability of the scheme is a challenging task because, similarly to finite element schemes, the stability constant depends on the geometry of the element and the polynomial degree of approximation.

We denote by N the number of elements in the mesh. To study the rate of convergence, we use the relations $\mathcal{O}(h) \approx \mathcal{O}(N^{-1/2})$. By $e(\cdot)$ we denote the error associated with the quantity $\cdot$ in its natural norm, and will denote by h_i the mesh size corresponding to a refinement level i. The experimental convergence order is computed as

$$r(\cdot) = \frac{\log(e_i(\cdot)) - \log(e_{i+1}(\cdot))}{\log(h_i) - \log(h_{i+1})} \approx -2\frac{\log(e_i(\cdot)) - \log(e_{i+1}(\cdot))}{(\log(N_i) - \log(N_{i+1}))},$$

where N_i and N_{i+1} are two consecutive measures of the number of elements for the refinements h_i and h_{i+1}, respectively.

When evaluating the performance of our numerical scheme, we explore different geometric configurations, thereby assessing its robustness and versatility. Triangle and quad meshes are generated using the DUNE mesher or the GMSH software [33] through the Pygmsh interface [42]. Voronoi and other polygonal meshes are constructed using Polymesher [43] and MATLAB, respectively.

For the experiments, we consider that the domain is partitioned considering the following types of meshes:

- $\mathcal{T}_{1,h}$:= A mesh using triangles;
- $\mathcal{T}_{2,h}$:= A mesh with quadrilaterals;
- $\mathcal{T}_{3,h}$:= A mesh with a Voronoi tessellation;
- $\mathcal{T}_{4,h}$:= A mesh with non-convex polygons.

Each of the above meshes contains convex polygons, except for $\mathcal{T}_{4,h}$. Considering each of them for the experiments has a slight effect on the sparsity pattern but it will affect the condition number of $\mathbf{A}$. More precisely, we note that the matrix $\mathbf{A}$ is a block matrix according to the discrete formulation given in Section 3. Now, let us consider the unit square domain $\Omega := (0,1)^2$, which will be frequently used throughout this section, and select a number of elements for each $\mathcal{T}_h$ such that the mesh sizes are similar. The sparsity pattern for each mesh is illustrated in Figure 2, where we observe slight variations between meshes, primarily due to the number of sides of the polygons and the total number of elements.

On the other hand, in Figure 3, we observe the behavior of the percentage of nonzero entries and the condition number. The results for the percentage of nonzero entries are expected due to the sparsity pattern observed above: as N increases, the number of zeros also increases. Moreover, we note that the condition number of the matrices with convex polygons $\mathcal{T}_{i,h}$, $i = 1,2,3$, grows with N, as expected. However, for $\mathcal{T}_{4,h}$, a considerable deterioration is observed. This behavior has been previously studied in [38], where it is shown that the ill-conditioning of the VEM scheme becomes evident when the typical monomial basis is used. This is the case of our scheme, but the numerical results remain satisfactory, as will be demonstrated below.

6.1. Convergence on a square domain

We start by considering the square domain $\Omega := (0,1)^2$ together with smooth solutions for the velocity and pressure. The right-hand side and boundary conditions are chosen such that the exact solutions are given by

$$\boldsymbol{u}(x,y) := \left(\frac{\partial\varphi}{\partial y}, -\frac{\partial\varphi}{\partial x}\right), \qquad p(x,y) := \sin(x-y),$$

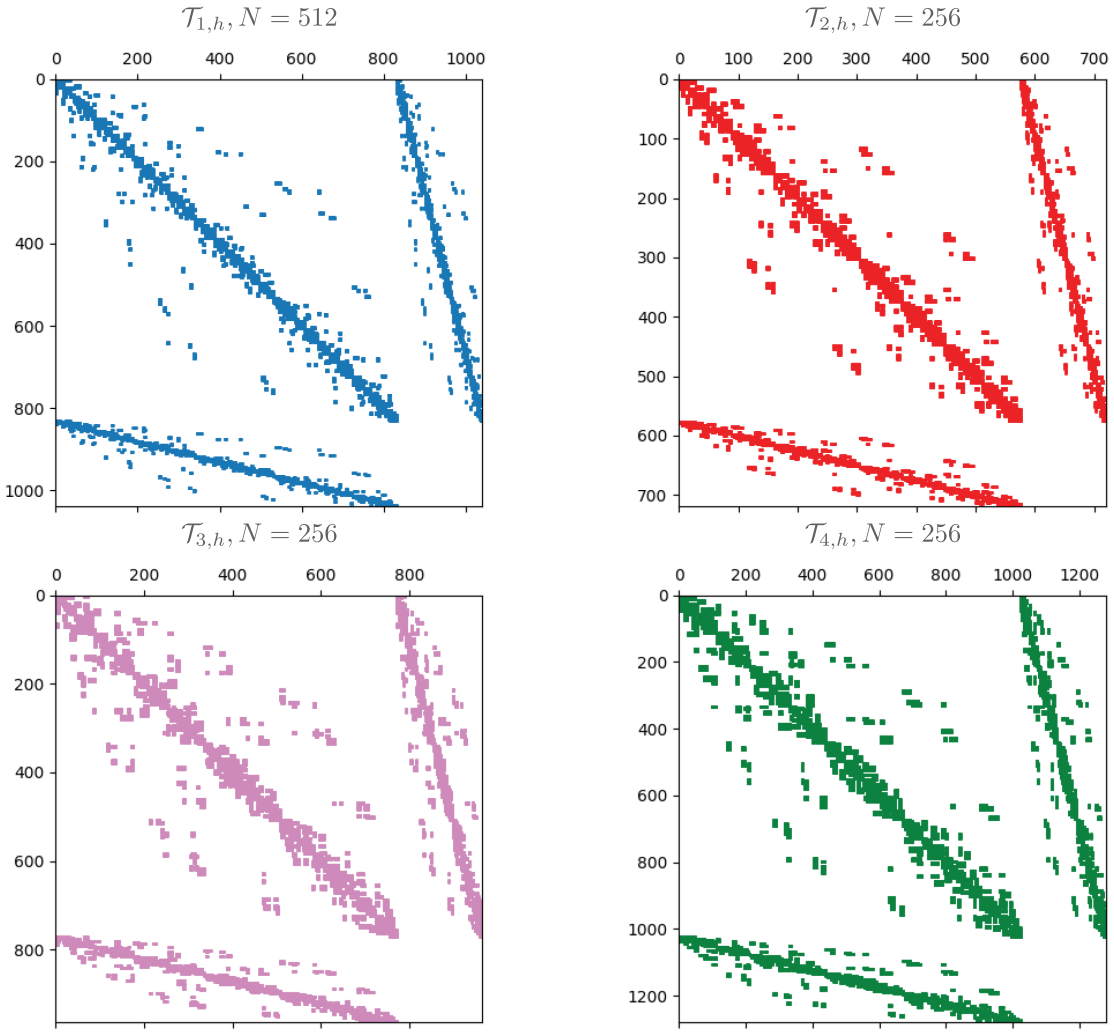

FIGURE 2. Sparsity pattern of $\mathbf{A}$ for different polygonal meshes in the unit square domain.

where $\varphi(x, y) := -256x^2(x-1)^2y(y-1)(2y-1)$. The velocity is solenoidal and is characterized by having non-zero tangential components across $y = 0$ and $y = 1$.

The error history, together with the values for the L^2-norm of $\nabla \cdot \boldsymbol{u}_h$ are presented in Tables 1 and 2. Here, we observe that the rates behave optimally through the different meshes, and the divergence of velocity is converging to zero. Also, we note that, although the choice of spaces is exactly divergence-free, this property is lost when using the proposed Nitsche's method. In fact, we observe that $\|\nabla \cdot \boldsymbol{u}_h\|_{0,\Omega}$ converges weakly to zero as $h \to 0$. For comparison, the error curves for $k = 2, 3$ are presented in Figure 4. We observe that the energy error behaves like $\mathcal{O}(h^k)$, as expected. Also, we note that the error is similar for different meshes with approximately same mesh-size at each iteration.

Figures 5 and 6 depict the velocity components and pressure surface plot. In Figure 5, we observe that the discrete solutions components agree with the proposed exact solution, independent of the mesh. Also, we note that the slip condition is properly imposed on $y = 0$ and $y = 1$. Figure 6 presents the pressure surface plot on different meshes, where no appreciable difference between them is observed.

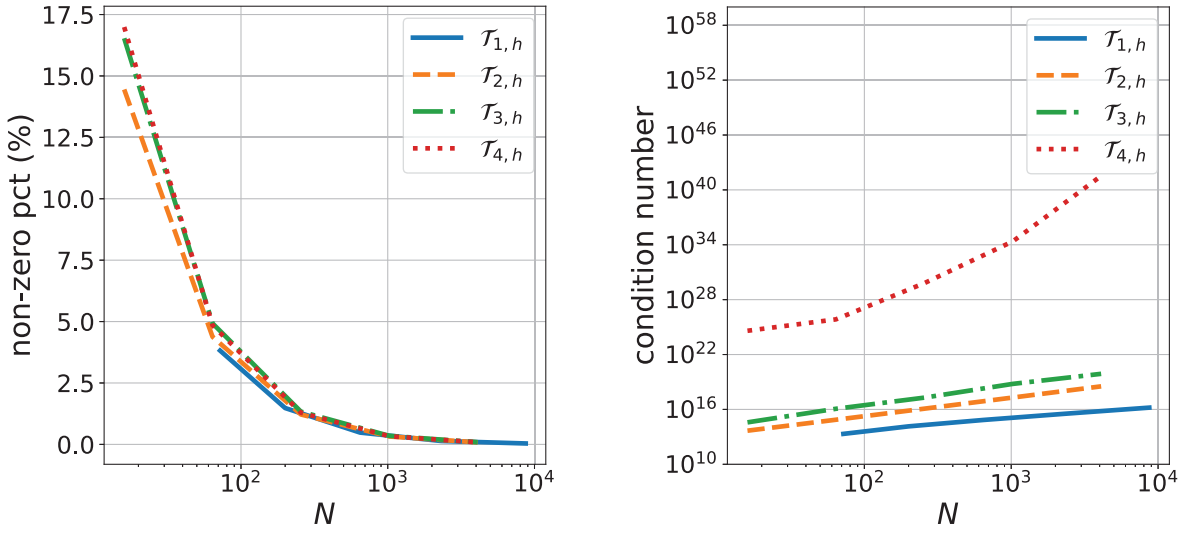

FIGURE 3. Non-zero percentage (left) and condition number (right) of the matrix $\mathbf{A}$ for different meshes.

TABLE 1. Example 6.1. Error history on different meshes with $k = 2$ for $\boldsymbol{u}_h$ and p_h on the unit square domain $\Omega = (0, 1)^2$.

$\mathcal{T}_{i,h}$	N	h	e($\boldsymbol{u}$)	$r(\boldsymbol{u})$	e(p)	$r(p)$	$\|\nabla \cdot \boldsymbol{u}_h\|_{0,\Omega}$
	128	0.177	1.94e+00	$\star$	7.98e−01	$\star$	1.47e−04
	512	0.088	6.16e−01	1.66	2.11e−01	1.92	2.69e−05
1	2048	0.044	1.79e−01	1.78	5.40e−02	1.97	5.01e−06
	8192	0.022	4.76e−02	1.91	1.36e−02	1.99	8.71e−07
	32 768	0.011	1.22e−02	1.97	3.41e−03	2.00	1.79e−07
	64	0.125	2.08e+00	$\star$	1.95e+00	$\star$	1.14e−03
	256	0.063	5.30e−01	1.97	5.61e−01	1.79	1.92e−04
2	1024	0.031	1.33e−01	1.99	1.50e−01	1.91	3.16e−05
	4096	0.016	3.33e−02	2.00	3.84e−02	1.96	5.51e−06
	16 384	0.008	8.32e−03	2.00	9.69e−03	1.99	1.07e−06
	64	0.162	2.01e+00	$\star$	1.28e+00	$\star$	7.39e−03
	256	0.089	4.85e−01	2.05	3.26e−01	1.97	8.47e−04
3	1024	0.046	1.28e−01	1.92	8.81e−02	1.89	1.24e−04
	4096	0.021	3.03e−02	2.08	1.91e−02	2.21	2.37e−05
	16 384	0.011	7.54e−03	2.01	4.51e−03	2.08	3.86e−06
	64	0.156	2.36e+00	$\star$	1.61e+00	$\star$	6.24e−03
	256	0.078	6.23e−01	1.93	4.54e−01	1.83	8.49e−04
4	1024	0.039	1.58e−01	1.98	1.18e−01	1.94	1.09e−04
	4096	0.020	3.97e−02	1.99	2.95e−02	2.00	1.35e−05
	16 384	0.010	9.94e−03	2.00	7.27e−03	2.02	1.59e−06

TABLE 2. Example 6.1. Error history on different meshes with $k = 3$ for $\boldsymbol{u}_h$ and p_h on the unit square domain $\Omega = (0,1)^2$.

$\mathcal{T}_{i,h}$	N	h	e($\boldsymbol{u}$)	$r(\boldsymbol{u})$	e(p)	$r(p)$	$\|\nabla \cdot \boldsymbol{u}_h\|_{0,\Omega}$
	128	0.177	2.00e−01	⋆	7.45e−02	⋆	3.03e−05
	512	0.088	2.42e−02	3.05	1.05e−02	2.83	3.89e−06
1	2048	0.044	2.96e−03	3.03	1.38e−03	2.93	1.14e−06
	8192	0.022	3.65e−04	3.02	1.76e−04	2.96	3.96e−07
	32 768	0.011	4.72e−05	2.95	2.23e−05	2.98	1.39e−07
	64	0.125	3.52e−01	⋆	2.15e−01	⋆	1.38e−04
	256	0.063	4.08e−02	3.11	3.57e−02	2.59	1.56e−05
2	1024	0.031	4.67e−03	3.13	5.04e−03	2.82	4.69e−06
	4096	0.016	5.47e−04	3.10	6.66e−04	2.92	1.66e−06
	16 384	0.008	6.56e−05	3.06	8.54e−05	2.96	5.88e−07
	64	0.162	2.67e−01	⋆	1.08e−01	⋆	1.36e−04
	256	0.089	3.39e−02	2.98	1.45e−02	2.89	8.00e−06
3	1024	0.046	4.63e−03	2.87	1.63e−03	3.16	1.71e−06
	4096	0.021	5.23e−04	3.15	1.56e−04	3.38	6.52e−07
	16 384	0.011	6.62e−05	2.98	1.77e−05	3.14	2.31e−07
	64	0.156	2.99e−01	⋆	1.54e−01	⋆	1.06e−04
	256	0.078	3.72e−02	3.01	2.15e−02	2.84	7.86e−06
4	1024	0.039	4.58e−03	3.02	2.74e−03	2.97	1.26e−06
	4096	0.020	5.65e−04	3.02	3.41e−04	3.00	4.12e−07
	16 384	0.010	7.01e−05	3.01	4.25e−05	3.01	1.46e−07

6.2. Robustness with respect to ν

In this section we aim to test the robustness of the scheme with respect to the viscosity. More precisely, we observe the error behavior when ν becomes small. For simplicity, the exact solutions are the ones given in Section 6.1, and we take $\mathcal{T} = \mathcal{T}_{3,h}$ (Voronoi mesh).

We consider a given viscosity $\nu = 10^{-3j}$, $j = 1, 2, 3, 4$, and $\mathbb{K} = \mathbb{I}$. The computed errors and experimental rates of convergence are given in Tables 3 and 4. We observe considerably small variations in the computed errors between taking $\nu = 10^{-3}$ and the rest, that do not affect the convergence rate. We also note that the divergence L^2-norm is the same for all the cases. A similar result was obtained when using the meshes $\mathcal{T}_{1,h}, \mathcal{T}_{2,h}$ and $\mathcal{T}_{4,h}$, confirming the theoretical robustness with respect to the viscosity predicted in Section 5.

6.3. Applications with several boundary conditions

This experiment aims to test the behavior of our method in applications where several boundary conditions are assumed. Let $\boldsymbol{g}_1$ and $\boldsymbol{g}_2$ be two vector fields such that

$$\boldsymbol{u} \cdot \boldsymbol{n} = \boldsymbol{g}_1 \cdot \boldsymbol{n}, \qquad (\boldsymbol{\varepsilon}(\boldsymbol{u}))\boldsymbol{n} \cdot \boldsymbol{t} = \boldsymbol{g}_2 \cdot \boldsymbol{t}, \qquad \text{on } \Gamma_N.$$

Then, the discrete right-hand sides forms with additional Nitsche terms are given as follow (cf. Sect. 3.1).

$$\widetilde{F}_h(\boldsymbol{v}_h) := F_h(\boldsymbol{v}_h) + \gamma_N \sum_{e \in \mathcal{E}_h^N} \int_e h_e^{-1} (\boldsymbol{g}_1 \cdot \boldsymbol{n})(\boldsymbol{v}_h \cdot \boldsymbol{n}) \, \mathrm{d}s - \sum_{e \in \mathcal{E}_h^N} \int_e \left(\boldsymbol{n}^t \left(\nu \boldsymbol{\varepsilon} \left(\Pi_{K_e}^{\boldsymbol{\varepsilon},k} \boldsymbol{v}_h \right) \boldsymbol{n} \right) \right) (\boldsymbol{g}_1 \cdot \boldsymbol{n}) \, \mathrm{d}s$$
$$+ \sum_{e \in \mathcal{E}_h^N} \int_e (\boldsymbol{g}_2 \cdot \boldsymbol{t})(\boldsymbol{v}_h \cdot \boldsymbol{t}) \, \mathrm{d}s$$

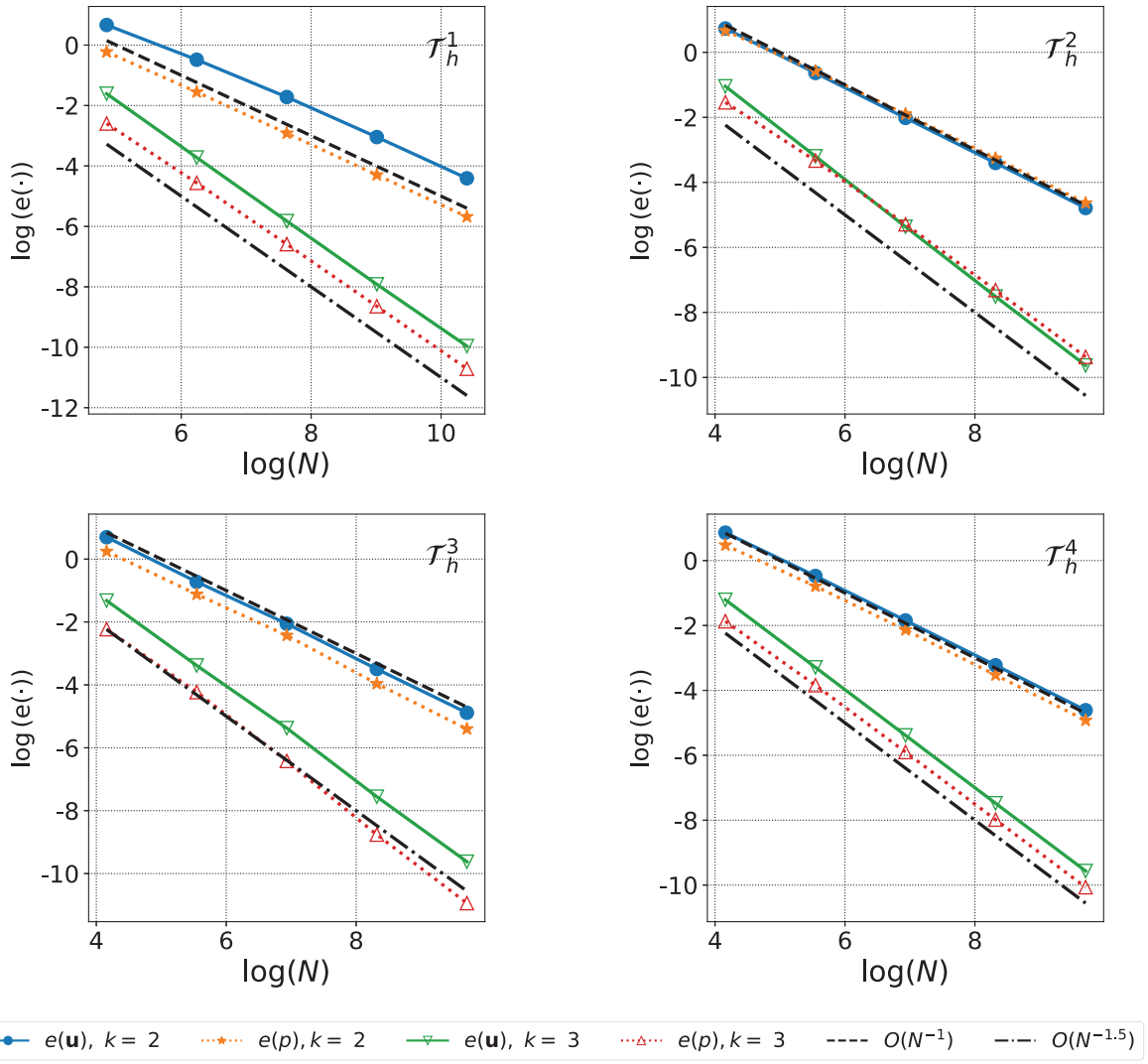

FIGURE 4. Example 6.1. Error curves of the virtual element scheme for the Brinkman equations using different meshes. Here, we set the parameters $\mathbb{K} = \mathbb{I}$, and $\nu = 1$.

$$\widetilde{G}(q_h) := G(q_h) + \sum_{e \in \mathcal{E}_h^N} \int_e \boldsymbol{g}_1 \cdot (q_h \boldsymbol{n}) \, \mathrm{d}s.$$

We divide the test in three cases, that we detail below.

6.3.1. Flow past cylinder

We first focus on the simulation of a cross-flow around a cylinder between two parallel plates. This phenomena can be characterized in a 2D model, for which we take $R = 0.05$ as the radius of the cylinder, and the length and height of the channel are given by $L = 0.82$ and $H = 0.41$, respectively. The resulting domain is of the form

$$\Omega := (0, L) \times (0, H) \backslash D_R(x_c, y_c),$$

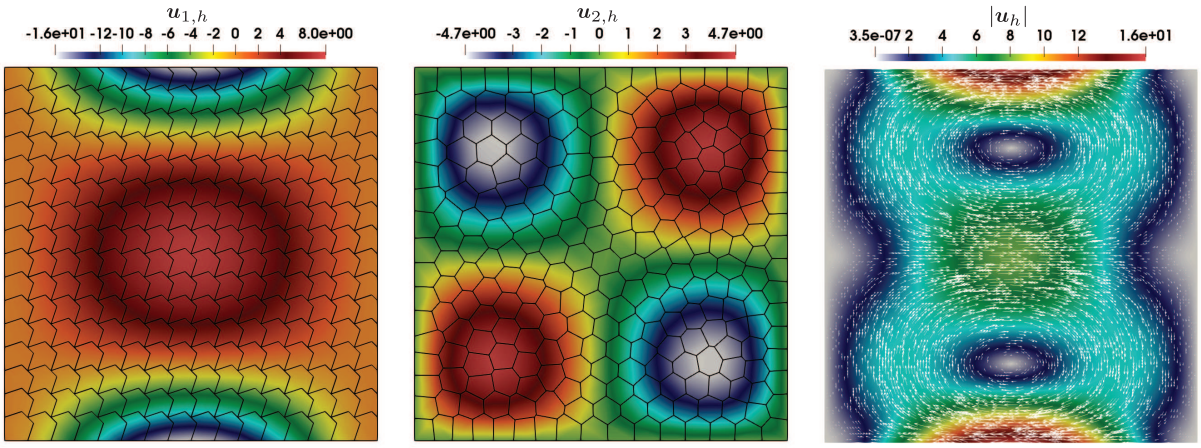

FIGURE 5. Example 6.1. Scalar components of the computed velocity $\boldsymbol{u}_{i,h}, i = 1, 2$ in different meshes together with the corresponding field $\boldsymbol{u}_h$.

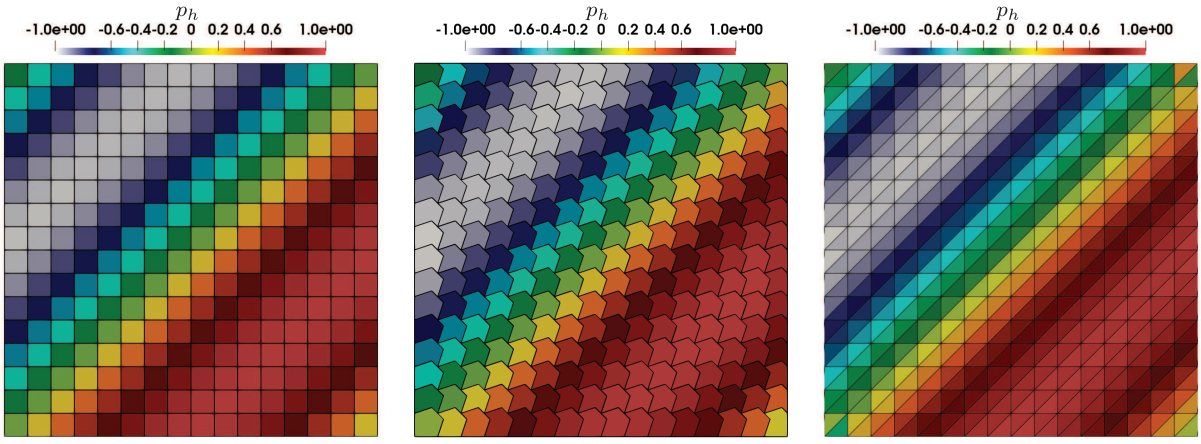

FIGURE 6. Example 6.1. Comparison between the computed pressure p_h on different polygonal meshes.

where D_R is the disk of radius R and centered at $(x_c, y_c) = (0.2, 0.2)$. We divide the boundaries as $\partial\Omega := \Gamma_{\text{in}} \cup \Gamma_{\text{wall}} \cup \Gamma_{\text{circ}} \cup \Gamma_{\text{out}}$, corresponding to the inlet, walls, inner circle and outlet boundary, respectively. Each of these subdomains have the following data:

$$\begin{aligned}
&\boldsymbol{u} = \boldsymbol{0}, && && \text{on } \Gamma_w \cup \Gamma_{\text{circ}},\\
&\boldsymbol{u}\cdot\boldsymbol{n} = \boldsymbol{g}_1\cdot\boldsymbol{n}, \quad (\nu\boldsymbol{\varepsilon}(\boldsymbol{u}))\boldsymbol{n}\cdot\boldsymbol{t} = \boldsymbol{g}_2\cdot\boldsymbol{t}, && \text{with } \boldsymbol{g}_1(x,y) = \left(\frac{6u_{\max}y(H-y)}{H^2}, 0\right)^{\mathtt{t}}, && \text{on } \Gamma_{\text{in}},\\
&(\nu\boldsymbol{\varepsilon}(\boldsymbol{u}) - p\mathbb{I})\boldsymbol{n} = \boldsymbol{0}, && && \text{on } \Gamma_{\text{out}},
\end{aligned}$$

and $\boldsymbol{g}_2(x, y) = \nu\boldsymbol{\varepsilon}(\boldsymbol{g}_1(x, y))\boldsymbol{n}$, with $u_{\max} = 2$. The viscosity is taken to be $\nu = 1$. Note that $\boldsymbol{g}_1$ corresponds to a Poiseuille flow and the condition over Γ_{out} is a free flow boundary condition. All the above conditions need a correct characterization of the traces on polygonal domains because we loose the $[H^1(\Omega)]^2$ condition of the velocity in a neighborhood of the corner points where Γ_w intersects Γ_{in}. Moreover, although the Nitsche

TABLE 3. Example 6.2. Error history with respect to different values of ν on the unit square domain for $\boldsymbol{u}_h$ and p_h. Here, we consider $k = 2$ as the scheme order.

ν	N	h	e($\boldsymbol{u}$)	$r(\boldsymbol{u})$	e(p)	$r(p)$	$\|\nabla \cdot \boldsymbol{u}_h\|_{0,\Omega}$
10^{-3}	64	0.162	2.19e+00	$\star$	9.48e−02	$\star$	7.04e−03
	256	0.089	4.95e−01	2.14	3.02e−02	1.65	8.14e−04
	1024	0.046	1.28e−01	1.96	6.72e−03	2.17	1.10e−04
	4096	0.021	3.03e−02	2.08	1.62e−03	2.05	1.92e−05
	16 384	0.011	7.54e−03	2.00	3.68e−04	2.14	1.10e−06
10^{-6}	64	0.162	2.37e+00	$\star$	9.40e−02	$\star$	7.04e−03
	256	0.089	5.61e−01	2.08	3.00e−02	1.65	8.14e−04
	1024	0.046	1.49e−01	1.91	6.66e−03	2.17	1.10e−04
	4096	0.021	3.37e−02	2.14	1.61e−03	2.05	1.92e−05
	16 384	0.011	8.27e−03	2.03	3.65e−04	2.14	1.10e−06
10^{-9}	64	0.162	2.37e+00	$\star$	9.40e−02	$\star$	7.04e−03
	256	0.089	5.61e−01	2.08	3.00e−02	1.65	8.14e−04
	1024	0.046	1.49e−01	1.91	6.66e−03	2.17	1.10e−04
	4096	0.021	3.39e−02	2.14	1.61e−03	2.05	1.92e−05
	16 384	0.011	8.44e−03	2.01	3.65e−04	2.14	1.10e−06
10^{-12}	64	0.162	2.37e+00	$\star$	9.40e−02	$\star$	7.04e−03
	256	0.089	5.61e−01	2.08	3.00e−02	1.65	8.14e−04
	1024	0.046	1.49e−01	1.91	6.66e−03	2.17	1.10e−04
	4096	0.021	3.39e−02	2.14	1.61e−03	2.05	1.92e−05
	16 384	0.011	8.44e−03	2.01	3.65e−04	2.14	1.10e−06

method proposed in this study works for curve boundaries, there is an inherent variational crime that needs the proposal of a Nitsche method on curved domains for Brinkman problems. These two facts are beyond the proposed theory.

We have depicted the computed velocity data in Figure 7. Here, we observe that the boundary conditions are applied correctly, having no-slip around the inner circle and the walls. Also, by comparing the plots of $\boldsymbol{u}_{1,h}$ and $\boldsymbol{u}_{2,h}$ in the outflow we observe that they are similar to that of a flow on a channel that ends at Γ_{out}. To observe the behavior at the inlet, we have also plotted in Figure 8 a comparison between the velocity profiles $\boldsymbol{u}_h \cdot \boldsymbol{n}|_{\Gamma_{\text{in}}} = \boldsymbol{g}_1 \cdot \boldsymbol{n}$ and $\boldsymbol{u}_h \cdot \boldsymbol{n}|_{\Gamma_{\text{in}}} = \boldsymbol{u}_{1,h}(0, y)$. Here, we observe that the parabolic profile is properly imposed by the scheme, and the zero-tangential stress yields the behavior observed for $\boldsymbol{u}_{2,h}(0, y)$. We observe a near-zero y-velocity at the middle of the channel with the highest values in the first and third quarters of the channel. Also, we observe that at the domain corner, a zero velocity is imposed. We finish this part of the experiment showing the surface plot of the pressure drop on two different meshes in Figure 9. A drop of gauge pressure from 1500 to -20 caused by the obstacle is observed, while the lowest values of the pressure are reached behind the obstacle and at the channel end. The negative pressure values are valid due to the incompressible formulation of the problem, which allows to write the variable p in terms of the gauge pressure. Finally, from the streamlines we note that there are no observable recirculation zones for the chosen parameters.

TABLE 4. Example 6.2. Error history with respect to different values of ν on the unit square domain for $\boldsymbol{u}_h$ and p_h. Here, we consider $k = 3$ as the scheme order.

ν	N	h	e($\boldsymbol{u}$)	$r(\boldsymbol{u})$	e(p)	$r(p)$	$\|\nabla \cdot \boldsymbol{u}_h\|_{0,\Omega}$
10^{-3}	64	0.162	2.74e−01	⋆	1.15e−02	⋆	1.02e−04
	256	0.089	2.96e−02	3.21	1.44e−03	3.00	7.42e−06
	1024	0.046	4.06e−03	2.87	1.59e−04	3.18	1.75e−06
	4096	0.021	5.01e−04	3.02	1.52e−05	3.38	6.56e−07
	16 384	0.011	6.54e−05	2.94	1.66e−06	3.20	2.32e−07
10^{-6}	64	0.162	3.47e−01	⋆	1.14e−02	⋆	1.02e−04
	256	0.089	4.45e−02	2.96	1.43e−03	3.00	7.42e−06
	1024	0.046	5.96e−03	2.90	1.58e−04	3.18	1.75e−06
	4096	0.021	6.80e−04	3.13	1.51e−05	3.38	6.56e−07
	16 384	0.011	8.09e−05	3.07	1.65e−06	3.20	2.32e−07
10^{-9}	64	0.162	3.47e−01	⋆	1.14e−02	⋆	1.02e−04
	256	0.089	4.46e−02	2.96	1.43e−03	3.00	7.42e−06
	1024	0.046	6.00e−03	2.89	1.58e−04	3.18	1.75e−06
	4096	0.021	6.93e−04	3.11	1.51e−05	3.38	6.56e−07
	16 384	0.011	8.68e−05	3.00	1.65e−06	3.20	2.32e−07
10^{-12}	64	0.162	3.47e−01	⋆	1.14e−02	⋆	1.02e−04
	256	0.089	4.46e−02	2.96	1.43e−03	3.00	7.42e−06
	1024	0.046	6.00e−03	2.89	1.58e−04	3.18	1.75e−06
	4096	0.021	6.93e−04	3.11	1.51e−05	3.38	6.56e−07
	16 384	0.011	8.68e−05	3.00	1.65e−06	3.20	2.32e−07

6.3.2. Flow into a backwards facing step

A classical benchmark test for the Stokes, Navier–Stokes or Brinkman equations is the backward facing step. Let us consider $H := 1$ and a channel given by

$$\Omega := (0, 9H) \times (0, 2H) \backslash \{(0, 2H) \times (0, H)\},$$

where we have a backward facing step in $(2H, H)$. We consider the left boundary as the inlet region with boundary conditions

$$\boldsymbol{u} \cdot \boldsymbol{n} = \boldsymbol{g}_1 \cdot \boldsymbol{n}, \quad (\nu \boldsymbol{\varepsilon}(\boldsymbol{u}))\boldsymbol{n} \cdot \boldsymbol{t} = \boldsymbol{g}_2 \cdot \boldsymbol{t}, \quad \text{with} \quad \boldsymbol{g}_1(x, y) = \big(u_{\max} - 0.5(y - 1.5H)^2, 0\big)^{\mathtt{t}},$$

and $\boldsymbol{g}_2(x, y)$ is given as in Section 6.3.1. As before, the inflow consists of a Poiseuille type flow, with $u_{\max} = 0.125$. At the outlet (right boundary), we impose a zero stress boundary condition $(\nu \boldsymbol{\epsilon}(\boldsymbol{u}) - p\mathbb{I})\boldsymbol{n} = \boldsymbol{0}$, and no-slip boundary conditions on the rest of $\partial\Omega$. The viscosity is taken to be $\nu = 1$. The experiment was carried in two different Voronoi meshes: one with 4096 elements, and the other with 16 384. The behavior for both meshes were similar, and we present the results with the coarsest mesh. The physical parameters were taken as $\mathbb{K} = \mathbb{I}$ and $\nu = 1$. The approximated velocity field and pressure are presented in Figure 10. Starting with the surface plot of $\boldsymbol{u}_{2,h}$, we note that a singularity is clearly visible at the reentrant corner, followed by a gradient of velocity at the outlet produced by the imposition of $(\nu \boldsymbol{\epsilon}(\boldsymbol{u}) - p\mathbb{I})\boldsymbol{n} = \boldsymbol{0}$. Next, we note that velocity field is that of a parabolic flow, with a recirculation zone captured by the velocity streamlines. Also, a drop of velocity magnitude from 0.12 to 0.05 is observed after the channel widens, which is also caused by pressure drop from 2.21 to 0.7. To observe the weak imposition of the boundary conditions at the inlet, we depict the velocity components in Figure 11, where we observe a good match between $\boldsymbol{g}_1 \cdot \boldsymbol{n}$ on Γ_{in} and $\boldsymbol{u}_{1,h}(0, y)$. The tangential component of the velocity, namely, $\boldsymbol{u}_{2,h}(0, y)$ shows a similar behavior to the one observed in Section 6.3.1.

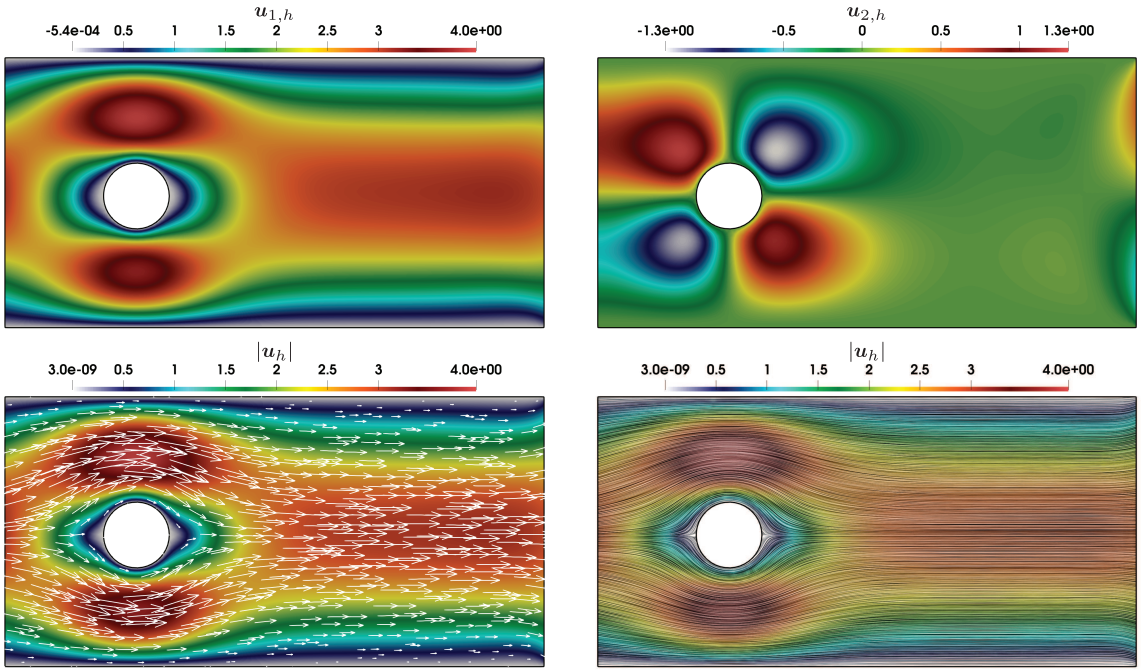

FIGURE 7. Example 6.3.1. Computed scalar components of the velocity field (top) along with the corresponding velocity field and streamlines (bottom) in the cross-flow model.

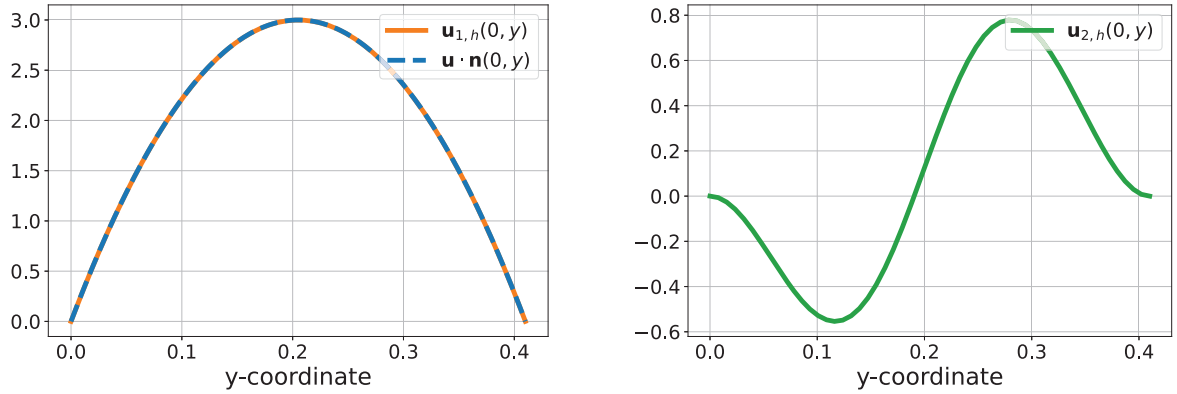

FIGURE 8. Example 6.3.1. Plots of the resulting computed inlet velocity components weakly imposed at Γ_{in}.

6.3.3. The lid-driven cavity flow

We end this section by performing the classical lid-driven cavity test where we model the steady flow of an immiscible fluid in a box. The aim of the test is to observe the physical changes of the medium when we modify the permeability parameter. We consider the unit square domain $\Omega = (0,1)^2$. The viscosity is taken to be $\nu = 10^{-3}$. The test is initially done with $\mathbb{K} = \kappa\mathbb{I}$, with $\kappa = 10^8$. We take $\Gamma_N = \emptyset$ and $\Gamma_D = \Gamma_{\text{wall}} \cup \Gamma_{\text{lid}}$, where Γ_{wall} corresponds to the bottom, left and right boundaries, and Γ_{lid} is the top boundary. We set $\boldsymbol{u}|_{\Gamma_{\text{lid}}} = (1,0)^{\mathtt{t}}$

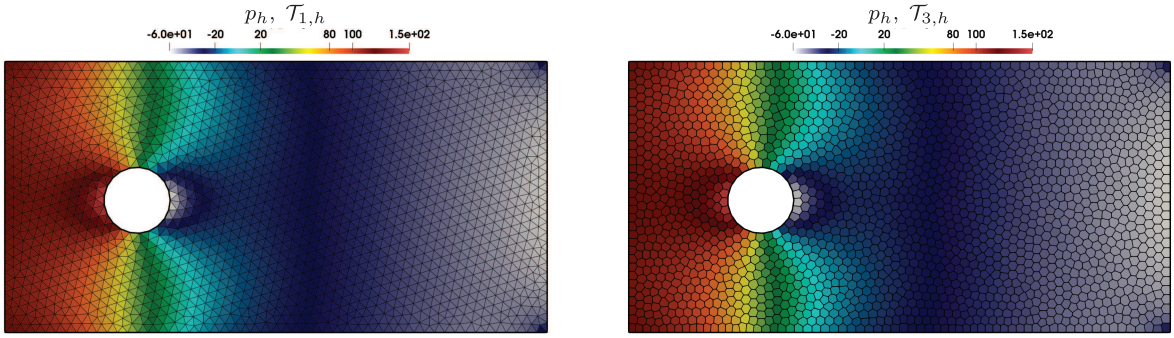

FIGURE 9. Example 6.3.1. Comparison between computed pressures in the cross-flow model using $\mathcal{T}_{1,h}$ and $\mathcal{T}_{3,h}$.

and $\boldsymbol{u}|_{\Gamma_{\text{wall}}} = \mathbf{0}$. We note that this type of boundary condition is also not covered by the theory because of the discontinuity of $\boldsymbol{u}$ on $\Gamma_{\text{lid}} \cap \Gamma_{\text{wall}}$.

The approximate velocities and pressure (displayed in Fig. 12) remain stable and corner singularities are clearly observed. The Nitsche scheme shows a good approximation of the boundary-discontinuous discrete function $\boldsymbol{u}_h$. Moreover, gradients of $\boldsymbol{u}_{2,h}$ and p_h are observed near the singularities.

Moreover, to assess the robustness of the method with respect to the choice of $\mathbb{K}$, we run several modified versions of this experiment by taking $\mathbb{K}^{-1} \in \{10^{-8}\mathbb{I}, 10\mathbb{I}, 10^2\mathbb{I}, 10^8\mathbb{I}\}$. More precisely, we are moving from a Stokes-dominated problem to a Darcy-dominated one. Plots of the streamlines of each case are presented in Figure 13. Here, we observe clear recirculation zones when we are on the Stokes-dominated version of the problem. As we start to decrease the permeability of the domain, the flow begins to flow near $y = 1$. In fact, when choosing $\mathbb{K}^{-1} = 10^8\mathbb{I}$, *i.e.*, a domain with very low permeability, we observe that the streamlines related to high velocity magnitudes are singularly concentrated along $y = 1$. In fact, the streamlines observed going down to the bottom of the domain for $\mathbb{K}^{-1} \in \{10\mathbb{I}, 10^2\mathbb{I}, 10^8\mathbb{I}\}$ correspond to small velocity magnitude with respect to the one imposed at Γ_{lid}. This example still serves as a benchmark to observe Nitsche's method to impose boundary conditions $\boldsymbol{u}|_{\Gamma_D}$ although we are dealing here with a limiting case, that is, the medium that behaves like an obstacle (impermeable medium).

7. CONCLUSIONS

In this work, we proposed a Nitsche-based virtual element method for the Brinkman problem with mixed boundary conditions, incorporating Dirichlet conditions on part of the boundary and slip conditions on the rest. The motivation for this approach arises from the challenges of strongly imposing slip boundary conditions in discrete settings due to the lack of degrees of freedom for normal components. By incorporating suitable Nitsche terms, we provided a symmetric variational formulation that weakly enforces these boundary conditions while ensuring stability and consistency.

The theoretical analysis established the well-posedness of the discrete problem through a global inf-sup condition, and we derived optimal convergence rates independent of the physical parameters. The numerical experiments further validated the method's robustness, demonstrating optimal accuracy and stability across various test cases. Additionally, the use of polygonal meshes highlights the flexibility of the virtual element framework in handling complex geometries. However, the proposed method exhibits only a weakly divergence-free behavior due to the extra terms introduced. Future research will focus on addressing this limitation, potentially by modifying the formulation to enforce stronger incompressibility constraints (see for example [18] and the references

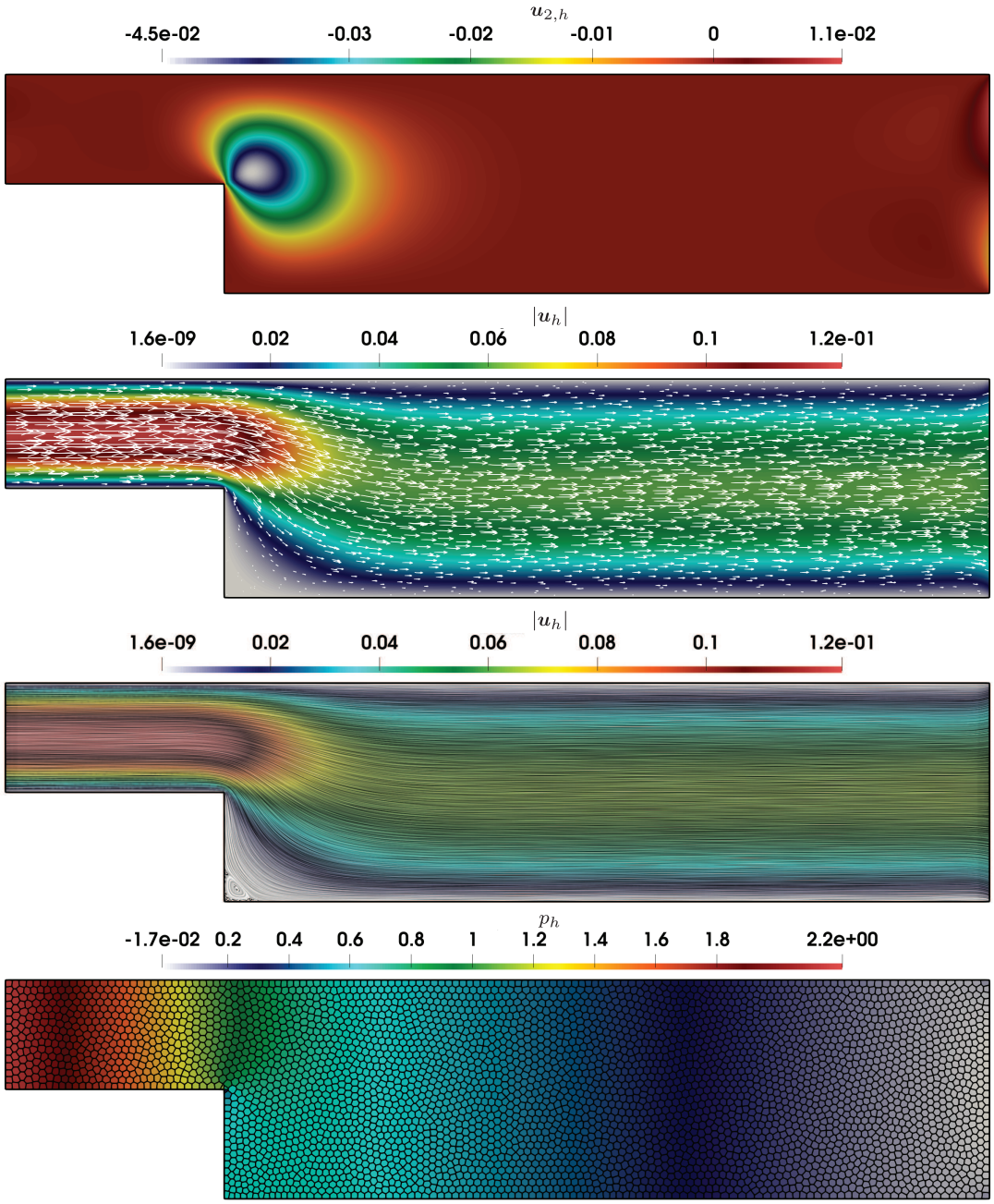

FIGURE 10. Example 6.3.2. Second velocity component (top) Velocity field streamlines (two in the middle) with pressure distribution (bottom), computed in a Voronoi mesh with 4096 elements.

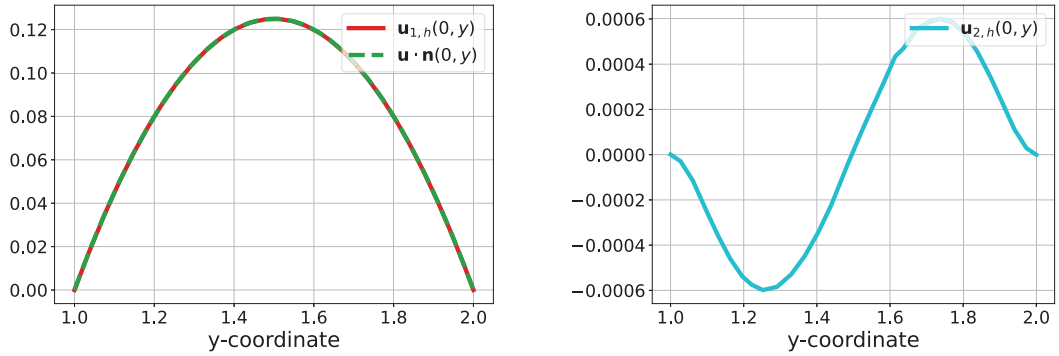

FIGURE 11. Example 6.3.2. Plots of the resulting computed inlet velocity components weakly imposed at the inlet for the flow into a backwards facing step.

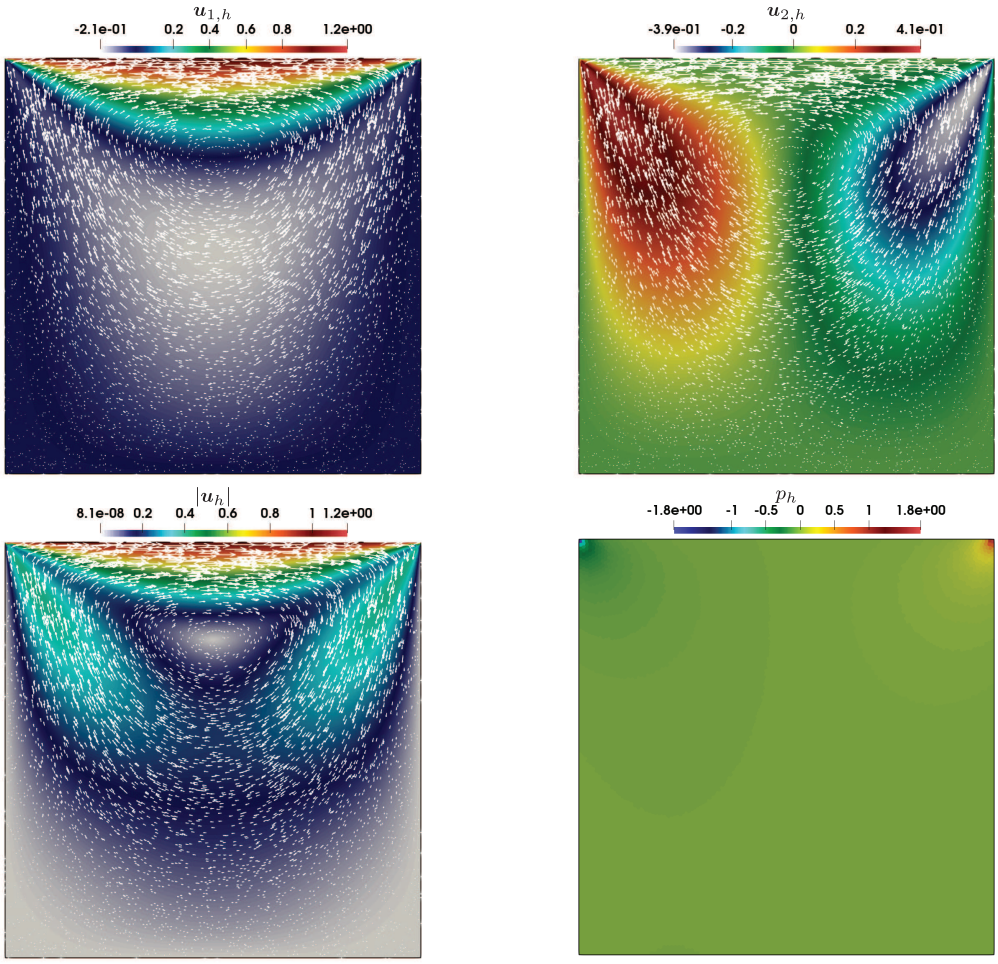

FIGURE 12. Example 6.3.3. Approximated velocity components and computed pressure on a Voronoi mesh for the lid-driven cavity test.

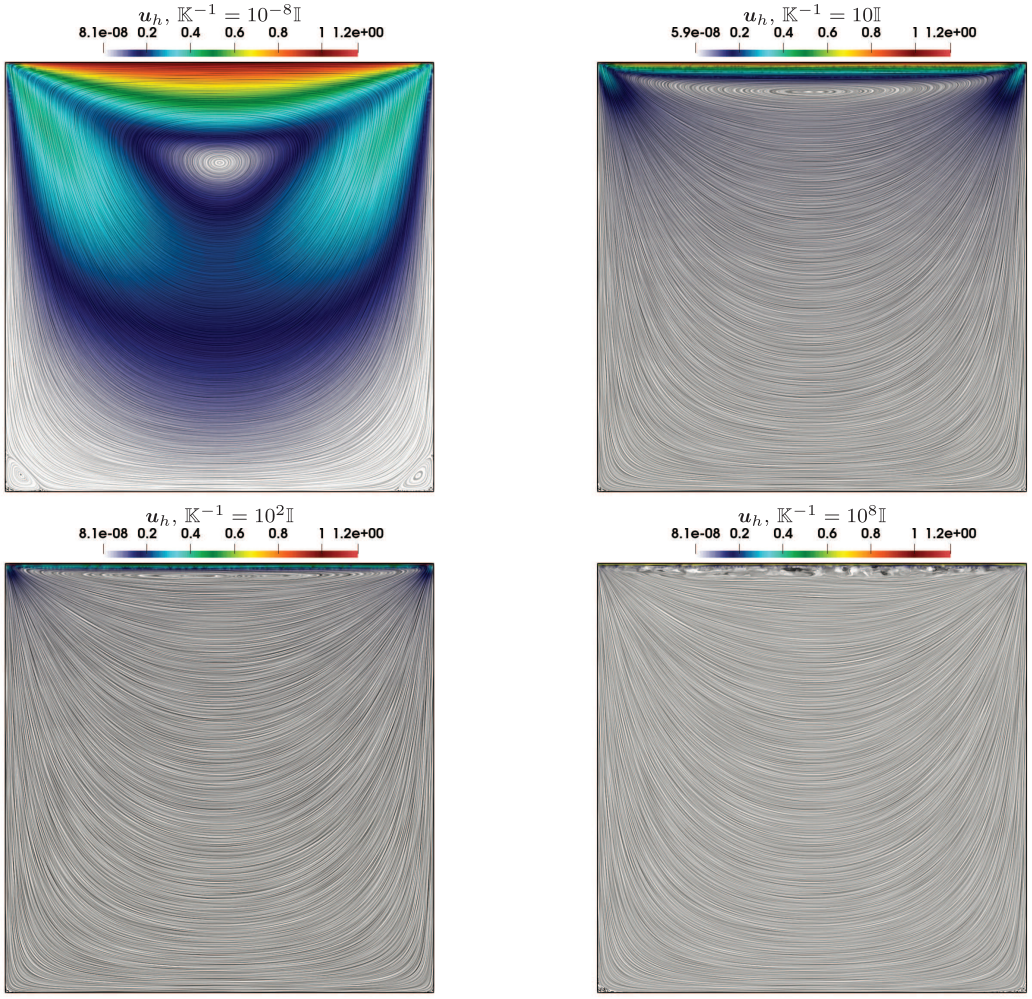

FIGURE 13. Example 6.3.3. Comparison of the velocity streamlines obtained for several values of $\mathbb{K}$ for the lid-driven cavity test. The color scale corresponds to $|\boldsymbol{u}_h|$.

therein). Further investigations into alternative stabilization techniques and extensions to more complex flow models will also be considered.

FUNDING

The authors have been partially supported by project Centro de Modelamiento Matemático (CMM), FB210005, BASAL funds for centers of excellence, and by the National Agency for Research and Development, ANID-Chile through project Anillo of Computational Mathematics for Desalination Processes ACT210087. The first author was partially supported by ANID-Chile through project FONDECYT 1220881. The second author was partially supported by the National Agency for Research and Development, ANID-Chile through FONDECYT Postdoctorado project 3230302. The third author was partially supported by the National Agency for Research and Development, ANID-Chile through FONDECYT Postdoctorado project 3240737.

CONFLICTS OF INTEREST

The authors have no conflicts of interest to declare.

Data availability statement

Enquiries about data availability should be directed to the authors.

References

[1] V. Anaya, D. Mora, R. Oyarzúa and R. Ruiz-Baier, A priori and a posteriori error analysis of a mixed scheme for the Brinkman problem. *Numer. Math.* **133** (2016) 781–817.

[2] V. Anaya, D. Mora and R. Ruiz-Baier, Pure vorticity formulation and Galerkin discretization for the Brinkman equations. *IMA J. Numer. Anal.* **37** (2017) 2020–2041.

[3] P.F. Antonietti, L. Beirão da Veiga, D. Mora and M. Verani, A stream virtual element formulation of the Stokes problem on polygonal meshes. *SIAM J. Numer. Anal.* **52** (2014) 386–404.

[4] P.F. Antonietti, C. Facciolà, P. Houston, I. Mazzieri, G. Pennesi and M. Verani, High-order discontinuous Galerkin methods on polyhedral grids for geophysical applications: seismic wave propagation and fractured reservoir simulations, in Polyhedral Methods in Geosciences. Vol. 27 of *SEMA SIMAI Springer Series*. Springer, Cham (2021) 159–225.

[5] P.F. Antonietti, L. Beirão da Veiga and G. Manzini, The Virtual Element Method and its Applications. Vol. 31. Springer (2022).

[6] H.J. Barbosa and T.J. Hughes, The finite element method with Lagrange multipliers on the boundary: circumventing the Babuška–Brezzi condition. *Comput. Methods Appl. Mech. Eng.* **85** (1991) 109–128.

[7] L. Beirão da Veiga, F. Brezzi, A. Cangiani, G. Manzini, L.D. Marini and A. Russo, Basic principles of virtual element methods. *Math. Models Methods Appl. Sci.* **23** (2013) 199–214.

[8] L. Beirão da Veiga, K. Lipnikov and G. Manzini, The Mimetic Finite Difference Method for Elliptic Problems. Vol. 11 of *MS&A. Modeling, Simulation and Applications*. Springer, Cham (2014).

[9] L. Beirão da Veiga, C. Lovadina and G. Vacca, Divergence free virtual elements for the Stokes problem on polygonal meshes. *ESAIM Math. Model. Numer. Anal.* **51** (2017) 509–535.

[10] L. Beirão da Veiga, C. Lovadina and G. Vacca, Virtual elements for the Navier–Stokes problem on polygonal meshes. *SIAM J. Numer. Anal.* **56** (2018) 1210–1242.

[11] L. Beirão da Veiga, D. Mora and G. Vacca, The Stokes complex for virtual elements with application to Navier–Stokes flows. *J. Sci. Comput.* **81** (2019) 990–1018.

[12] L. Beirão da Veiga, F. Brezzi, L.D. Marini and A. Russo, The virtual element method. *Acta Numer.* **32** (2023) 123–202.

[13] L. Beirão da Veiga, C. Lovadina and M. Trezzi, CIP-stabilized virtual elements for diffusion-convection-reaction problems. *IMA J. Numer. Anal.* **45** (2024) 934–970.

[14] S. Bertoluzza, M. Pennacchio and D. Prada, Weakly imposed Dirichlet boundary conditions for 2D and 3D Virtual Elements. *Comput. Methods Appl. Mech. Eng.* **400** (2022) 115454.

[15] D. Boffi, F. Brezzi and M. Fortin, Mixed Finite Element Methods and Applications. Vol. 44. Springer (2013).

[16] L. Botti, D.A. Di Pietro and J. Droniou, A Hybrid High-Order discretisation of the Brinkman problem robust in the Darcy and Stokes limits. *Comput. Methods Appl. Mech. Eng.* **341** (2018) 278–310.

[17] S.C. Brenner and L.R. Scott, The Mathematical Theory of Finite Element Methods. Springer (2008).

[18] E. Burman, P. Hansbo and M. Larson, Cut finite element method for divergence-free approximation of incompressible flow: a lagrange multiplier approach. *SIAM J. Numer. Anal.* **62** (2024) 893–918.

[19] E. Cáceres and G.N. Gatica, A mixed virtual element method for the pseudostress-velocity formulation of the Stokes problem. *IMA J. Numer. Anal.* **37** (2017) 296–331.

[20] E. Cáceres, G.N. Gatica and F.A. Sequeira, A mixed virtual element method for the Brinkman problem. *Math. Models Methods Appl. Sci.* **27** (2017) 707–743.

[21] A. Cangiani, E.H. Georgoulis and P. Houston, *hp*-version discontinuous Galerkin methods on polygonal and polyhedral meshes. *Math. Models Methods Appl. Sci.* **24** (2014) 2009–2041.

[22] N. Carro, D. Mora and J. Vellojin, A finite element model for concentration polarization and osmotic effects in a membrane channel. *Int. J. Numer. Methods Fluids* **96** (2024) 601–625.

[23] F. Chouly and P. Hild, A Nitsche-based method for unilateral contact problems: numerical analysis. *SIAM J. Numer. Anal.* **51** (2013) 1295–1307.

[24] F. Chouly, R. Mlika and Y. Renard, An unbiased Nitsche's approximation of the frictional contact between two elastic structures. *Numer. Math.* **139** (2018) 593–631.

[25] A. Dedner and A. Hodson, A framework for implementing general virtual element spaces. *SIAM J. Sci. Comput.* **46** (2024) B229–B253.

[26] A. Dedner, R. Klöfkorn, M. Nolte and M. Ohlberger, A generic interface for parallel and adaptive discretization schemes: abstraction principles and the DUNE-FEM module. *Computing* **90** (2010) 165–196.

[27] D.A. Di Pietro and J. Droniou, The Hybrid High-Order Method for Polytopal Meshes. Vol. 19 of *MS&A. Modeling, Simulation and Applications: Design, Analysis and Applications*. Springer, Cham (2020).

[28] D.A. Di Pietro and J. Droniou, A polytopal method for the Brinkman problem robust in all regimes. *Comput. Methods Appl. Mech. Eng.* **409** (2023) 115981.

[29] D.A. Di Pietro and A. Ern, A hybrid high-order locking-free method for linear elasticity on general meshes. *Comput. Methods Appl. Mech. Eng.* **283** (2015) 1–21.

[30] L.F. Gatica and F.A. Sequeira, A priori and a posteriori error analyses of an HDG method for the Brinkman problem. *Comput. Math. Appl.* **75** (2018) 1191–1212.

[31] G.N. Gatica and F.A. Sequeira, An L^p spaces-based mixed virtual element method for the two-dimensional Navier–Stokes equations. *Math. Models Methods Appl. Sci.* **31** (2021) 2937–2977.

[32] G.N. Gatica, M. Munar and F.A. Sequeira, A mixed virtual element method for a nonlinear Brinkman model of porous media flow. *Calcolo* **55** (2018) 21.

[33] C. Geuzaine and J.-F. Remacle, Gmsh: a 3-D finite element mesh generator with built-in pre-and post-processing facilities. *Int. J. Numer. Methods Eng.* **79** (2009) 1309–1331.

[34] I. Gjerde and L. Scott, Nitsche's method for Navier–Stokes equations with slip boundary conditions. *Math. Comput.* **91** (2022) 597–622.

[35] P. Hansbo, Nitsche's method for interface problems in computational mechanics. *GAMM-Mitteilungen* **28** (2005) 183–206.

[36] X. Huang and F. Wang, Analysis of divergence free conforming virtual elements for the Brinkman problem. *Math. Models Methods Appl. Sci.* **33** (2023) 1245–1280.

[37] M. Juntunen and R. Stenberg, Nitsche's method for general boundary conditions. *Math. Comput.* **78** (2009) 1353–1374.

[38] L. Mascotto, Ill-conditioning in the virtual element method: stabilizations and bases. *Numer. Methods Part. Differ. Equ.* **34** (2018) 1258–1281.

[39] S. Meddahi and R. Ruiz-Baier, A new DG method for a pure-stress formulation of the Brinkman problem with strong symmetry. *Netw. Heterog. Media* **17** (2022) 893–916.

[40] D. Mora, C. Reales and A. Silgado, A C^1-virtual element method of high order for the Brinkman equations in stream function formulation with pressure recovery. *IMA J. Numer. Anal.* **42** (2022) 3632–3674.

[41] J. Nitsche, Über ein variationsprinzip zur lösung von dirichlet-problemen bei verwendung von teilräumen, die keinen randbedingungen unterworfen sind, in Abhandlungen aus dem mathematischen Seminar der Universität Hamburg. Vol. 36. Springer (1971) 9–15.

[42] N. Schlömer, pygmsh: a Python frontend for Gmsh. Zenodo (2021).

[43] C. Talischi, G.H. Paulino, A. Pereira and I.F. Menezes, Polymesher: a general-purpose mesh generator for polygonal elements written in Matlab. *Struct. Multidisciplinary Optim.* **45** (2012) 309–328.

[44] J.M. Urquiza, A. Garon and M.-I. Farinas, Weak imposition of the slip boundary condition on curved boundaries for stokes flow. *J. Comput. Phys.* **256** (2014) 748–767.

[45] G. Vacca, An H^1-conforming virtual element for Darcy and Brinkman equations. *Math. Models Methods Appl. Sci.* **28** (2018) 159–194.

[46] P. Virtanen, R. Gommers, T.E. Oliphant, M. Haberland, T. Reddy, D. Cournapeau, E. Burovski, P. Peterson, W. Weckesser, J. Bright, S.J. van der Walt, M. Brett, J. Wilson, K.J. Millman, N. Mayorov, A.R.J. Nelson, E. Jones, R. Kern, E. Larson, C.J. Carey, İ. Polat, Y. Feng, E.W. Moore, J. VanderPlas, D. Laxalde, J. Perktold, R. Cimrman, I. Henriksen, E.A. Quintero, C.R. Harris, A.M. Archibald, A.H. Ribeiro, F. Pedregosa, P. van Mulbregt and SciPy 1.0 Contributors, SciPy 1.0: fundamental algorithms for scientific computing in python. *Nat. Methods* **17** (2020) 261–272.

[47] P. Wriggers, M. De Bellis and B. Hudobivnik, A Taylor–Hood type virtual element formulations for large incompressible strains. *Comput. Methods Appl. Mech. Eng.* **385** (2021) 114021.

[48] L. Zhao, E. Chung and M.F. Lam, A new staggered DG method for the Brinkman problem robust in the Darcy and Stokes limits. *Comput. Methods Appl. Mech. Eng.* **364** (2020) 112986.